DISSERTATIONES
TECHNOLOGIAE
UNIVERSITATIS
TARTUENSIS
99

MART ERNITS

Microfluidic production and characterization of liposomes towards localized payload release

DISSERTATIONES TECHNOLOGIAE UNIVERSITATIS TARTUENSIS
99

DISSERTATIONES TECHNOLOGIAE UNIVERSITATIS TARTUENSIS
99

MART ERNITS

Microfluidic production and characterization of liposomes towards localized payload release

UNIVERSITY OF TARTU
Press
1632

Institute of Technology, Faculty of Science and Technology, University of Tartu, Estonia

The dissertation was accepted for the commencement of the degree of Doctor of Philosophy in Biomedical Technology on 10.04.2026, by the Joint Council of the Doctoral Program of Engineering and Technology of the University of Tartu.

Supervisors: Veikko Pentti Linko, PhD
Associate Professor of Molecular Nanotechnology
Institute of Technology, University of Tartu, Estonia

Veronika Zadin, PhD
Professor of Materials Technology
Institute of Technology, University of Tartu, Estonia

Andreas Kyritsakis, PhD
Associate Professor of Multi-Scale Simulations
Institute of Technology, University of Tartu, Estonia

Olavi Reinsalu, PhD
Research Fellow in Molecular Nanotechnology
Institute of Technology, University of Tartu, Estonia

Reviewer: Kaido Kurrikoff, PhD
Associate Professor of Molecular Biotechnology
Institute of Technology, University of Tartu, Estonia

Opponent: Fernando Benito López, PhD
Associate Professor, Vice-Rector for Faculty and Research
EUNEIZ University, Spain

Commencement: Auditorium 121, Nooruse 1, Tartu, Estonia, at 14.15 on May 28th, 2026

Publication of this thesis is granted by the Institute of Technology, Faculty of Science and Technology, University of Tartu.

ISSN 2228-0855 (print)
ISBN 978-9908-57-199-7 (print)
ISSN 2806-2620 (pdf)
ISBN 978-9908-57-200-0 (pdf)

Copyright: Mart Ernits, 2026

University of Tartu Press
www.tyk.ee

ABSTRACT

Drug delivery and release can increase therapeutic index by reducing the amount of drug interactions with healthy tissues. Liposomes are a promising carrier type for drug delivery and release. This thesis develops a microfluidic and analytical toolkit to fabricate and characterize liposomes on multiple size ranges toward externally triggered release. Giant unilamellar vesicles (GUVs) were produced using octanol-assisted liposome assembly (OLA), which enabled controlled encapsulation of diverse cargo including enhanced green fluorescent protein (eGFP) and magnetic microspheres, while yielding narrow size distributions (mean diameter of GUV $92 \pm 6\,\mu$m). Stability and passive permeability were tested by time-lapse counting and a calcein release assay, showing an exponential loss of visible vesicles with 90% payload release within 24 h. To obtain more stable carriers, small unilamellar vesicle (SUV) and large unilamellar vesicle (LUV) were generated by hydrodynamic focusing. Dynamic light scattering (DLS) and transmission electron microscopy (TEM) confirmed the presence of multimodal liposome populations with diameters at about ≈ 80 nm, ≈ 180 nm and ≈ 420 nm. The nanoscale liposomes exhibited considerably higher stability compared to the GUVs, with the particle concentration decreasing only $\approx 5\%$ over four days in an experiment where the peaks of the liposome size distribution were measured to be at ≈ 200 nm and ≈ 430 nm. To support reproducible microfluidic liposome production, a four-channel piezoelectric pressure controller and companion software, pressure controller software, were engineered, providing a ± 1000 mbar operating range with $< 0.7\%$ reporting error versus a calibrated manometer and typically 3–10 s transitions between setpoints, at a feasible cost. Finally, a software named *EasyFlow* was developed to streamline post-image analysis for droplet and vesicle experiments, enabling threshold-based classification, polydisperse analysis, as well as growth heterogeneity metrics compatible with high-throughput workflows. Collectively, these methods establish a robust platform for future studies of magnetically responsive liposomes which could find uses in spatially localized, externally triggered payload release.

CONTENTS

LIST OF ORIGINAL PUBLICATIONS

Publications included in the thesis

- **Paper I: M. Ernits**, O. Reinsalu, N. Yandrapalli, S. Kopanchuk, E. Moradpur-Tari, I. Sanka, O. Scheler, A. Rinken, R. Kurg, A. Kyritsakis*, V. Linko*, and V. Zadin*. "Microfluidic production, stability and loading of synthetic giant unilamellar vesicles". *Scientific Reports* 14 (2024), #14071. https://doi.org/10.1038/s41598-024-64613-4.
- **Paper II: M. Ernits***, O. Reinsalu, A. Kyritsakis, V. Linko*, and V. Zadin*. "Low-Cost, Open-Source, High-Precision Pressure Controller for Multi-Channel Microfluidics". *Biosensors* 15.3 (2025) #154. https://doi.org/10.3390/bios15030154.
- **Paper III:** I. Sanka, S. Bartkova, P. Pata, **M. Ernits**, M. M. Meinberg, N. Agu, V. Aruoja, O.-P. Smolander*, and O. Scheler*. "User-friendly analysis of droplet array images". *Analytica Chimica Acta* 1272 (2023), #341397. https://doi.org/10.1016/j.aca.2023.341397.

Publications not included in the thesis

- O. Reinsalu*, **M. Ernits**, and V. Linko*. "Liposome-based hybrid drug delivery systems with DNA nanostructures and metallic nanoparticles". *Expert Opinion on Drug Delivery* 21.6 (2024), pp. 905–920. https://doi.org/10.1080/17425247.2024.2375389.
- E. Moradpur-Tari*, S. Vlassov, S. Oras, **M. Ernits**, E. Damerchi, B. Polyakov, A. Kyritsakis, and V. Zadin. "Nano1D: An accurate computer vision software for analysis and segmentation of low-dimensional nanostructures". *Ultramicroscopy* 261 (2024), #113949. https://doi.org/10.1016/j.ultramic.2024.113949.

Author's contribution to the publications

- **Paper I:** Designed and performed the main experiments. The manuscript was written and revised through contributions of all authors.
- **Paper II:** Designed and built the pressure controller and performed the main experiments. The manuscript was written and revised through contributions of all authors.
- **Paper III:** Participated in the development of the "EasyFlow" data processing tool for particle analysis and contributed to the manuscript revision process.

*Corresponding author.

LIST OF ABBREVIATIONS

Acronyms

ADC analog to digital converter 43, 44

CCD charge coupled device 31
CRISPR Clustered Regularly Interspaced Short Palindromic Repeats 39

DAC digital to analog converter 44
DLS dynamic light scattering 32, 33, 55, 56
DPPC dipalmitoylphosphatidylcholine 35, 55
DPPG dipalmitoylphosphatidylglycerol 14, 15, 35, 55
DSPC 1,2-distearoyl-sn-glycero-3-phosphocholine 14

eGFP enhanced green fluorescent protein 34, 37, 51, 53, 54
EM electron microscopy 30, 31
EV extracellular vesicle 13, 19

FS full scale 46, 49

GUI graphical user interface 41–43, 47
GUV giant unilamellar vesicle 13, 16–19, 28–30, 33, 34, 36–38, 41, 45, 50–57, 59

HDF hydrodynamic focusing 16–18, 28, 33, 35, 41, 45, 55, 56, 59, 60

IA inner aqueous phase 16, 33, 34, 38, 50, 53
IC inhibitory concentration 26

LC Liposome counter 36, 37, 51, 53, 56
LNP lipid nanoparticle 13, 21
LO lipid-oil 16, 33, 34, 42, 50, 59
LUV large unilamellar vesicle 13, 55, 57

MIC minimum inhibitory concentration 26, 27, 40
MRI magnetic resonance imaging 20
MUV medium unilamellar vesicle 13

OA outer aqueous phase 16, 33, 34
OLA octanol-assisted liposome assembly 16–18, 30, 33, 34, 41, 42, 48, 50, 52, 53, 55, 59, 60

PA phosphatidic acid 14
PC phosphatidylcholine 14
PCR polymerase chain reaction 21, 25
PCS pressure controller software 41, 43, 47
PDADMAC polydiallyldimethylammonium chloride 34, 50
PDI polydispersity index 32, 33, 51, 53, 55
PDMS polydimethylsiloxane 24, 25, 35
PE phosphatidylethanolamine 14
PEG polyethylene glycol 18
PEPC piezoelectric pressure controller 41–50, 55, 56, 59
PID proportional-integral-differential 23, 25, 44, 47
POPC 1-palmitoyl-2-oleoyl-sn-glycero-3-phosphocholine 14, 15, 33, 50, 52, 55
PS phosphatidylserine 14
PSS polystyrene sulfonate 34, 50
PTFE polytetrafluoroethylene 33

SD standard deviation 46, 47, 51, 54
SPION superparamagnetic iron oxide nanoparticle 19, 20
SUV small unilamellar vesicle 13, 28, 29, 31, 55–57

TEM transmission electron microscopy 30, 31, 35, 55
TFF tangential flow filtering 35, 55
TFH thin film hydration 16–18, 60
TI therapeutic index 11, 19
TRL technology readiness level 27

USB universal serial bus 41, 42, 44

1. INTRODUCTION

1.1. Drug delivery and release

Cancer has been found to be the cause for 16.8% of all deaths in the world in the 21st century [22]. It is a very difficult disease to treat because of the wide variety of mechanisms for its emergence and the fact that the pathogenic cells are difficult to distinguish from healthy ones. For over a century, scientists have been searching for a way to transport a drug precisely to the intended site to minimize side effects. Paul Ehrlich was the first to clearly articulate this concept and he coined the term *magic bullet* for it in 1908 [11, 158, 129]. The proposed mechanism involved chemical recognition of targets on the surfaces of pathogenic and diseased entities, which is similar to the way the adaptive immune system operates (T and B-cells recognize specific antigens). Over time, many chemical targeting methods have been developed, for example folate receptor targeting using drugs or folic acid conjugated drug carriers and also antibody-drug conjugates [130, 17]. Additionally, there are other methods besides chemical targeting. For example, mesoporous silica nanoparticles [66] or polymeric nanoparticles [69] and liposomes [76] can be loaded with drugs, and they will naturally degrade and release the drugs inside (acidic) tumor microenvironments. If the pathogen is not easily recognizable, the "bullet" may fail to reach the correct target, reducing its effectiveness. This can result in a low ratio of the median toxic dose to the median effective dose. This ratio is known as the therapeutic index (TI). [132, 52] To increase the TI, drug delivery methods using carriers that have been engineered to release the drug only at the site of interest have been proposed. Although chemical recognition of targets remains the most common method, spatial targeting has also been explored. These approaches have the potential to enhance the therapeutic index and reduce the required dose to treat patients. [11, 107, 137, 158]

The terms drug delivery and drug release are sometimes used interchangeably in the literature, e.g., delivery is described in terms of release kinetics [2] and release is used to denote site-specific delivery to tumors [27, 82]. However, there is a clear distinction between the two. Drug delivery denotes the process of transporting a therapeutic agent to the site of action within the body. Drug release is a sub-process that specifically denotes the liberation of an active drug from a disabling system, enabling it to exert its therapeutic effect at the target site.

In addition to drug delivery, it is also important to consider drug release kinetics because they affect the rate of drug adsorption and duration of circulation in the patient before it is used up or expelled from the system. Ideally, drugs should not be administered continuously, but rather periodically or even just once. This way, the patients can live their lives more normally, and there is also less labor required from the medical staff. [42, 85, 89]

1.2. Vesicles and liposomes

As noted earlier, various types of carriers can serve to deliver drugs to target sites. Among these, liposomes and other vesicular systems are particularly versatile. They are synthetic spherical structures made of phospholipids that are designed to mimic some properties, such as the separation of the inner and outer space, of naturally occurring vesicles that have lipid bilayers (Figure 1).

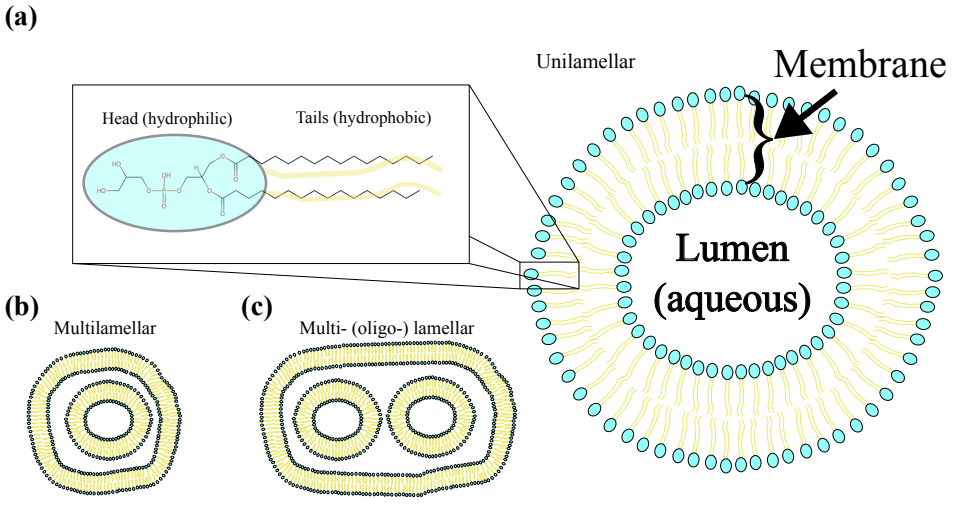

Figure 1: Cross-sectional schematic views of liposomes. The blue dots represent hydrophilic heads and yellow squiggles represent hydrophobic tails of phospholipid molecules. The liposome membrane separates the inner aqueous liquid (lumen) from the outer aqueous environment. (a) Unilamellar liposome. (b and c) Multilamellar liposomes.

The hydrophobic tails face towards each other (inward), while the hydrophilic head groups are oriented towards the surrounding aqueous environment, forming a (bilayered) membrane. This membrane forms a boundary between the inner (lumen) and the outer aqueous media.

The thickness of a biological membrane is typically about 4–5 nm (18-carbon acyl chain), but membranes can also be thicker in the case of long-chain phospholipids. This thickness also affects the maximum diameter of the particles that can be embedded into the membrane, for example, when producing magnetic liposomes (Section 1.2.4). For instance, spherical particles with 11 nm diameter can only be incorporated into the membrane in the presence of longer chain (24 carbon atoms) phospholipids. However, particles with a diameter of 7 nm can fit inside membranes even when the membrane is comprised of only 18-carbon-chain phospholipids. [87]

An important structural parameter of liposomes is lamellarity, which refers to the number of concentric phospholipid bilayers. Unilamellar vesicles contain a single bilayer (Figure 1a). In contrast, multilamellar vesicles consist of multiple

bilayers, either nested within one another (Figure 1b) or arranged as a single liposome encapsulating smaller ones (Figure 1c). [32, 115] Unilamellar liposomes are further categorized by size: giant unilamellar vesicles (GUVs) have a diameter greater than 1 μm, medium/large unilamellar vesicles (MUVs/LUVs) range between 100 nm and 1 μm, and small unilamellar vesicles (SUVs) are less than 100 nm in diameter. [115]

In biological systems, vesicles are membrane-bound compartments formed by cells both internally and externally to perform various functions, such as transport of nutrients, waste disposal, and cell-to-cell signaling. These natural particles were discovered gradually over the course of several decades. The first electron microscopy images of particles that we now know as vesicles were published in 1967 by Peter Wolf, who called them platelet dust. [151, 56, 28]

In the early twenty-first century, research on extracellular vesicles (EVs), which are vesicles that are usually formed by cells that eject parts of their cytoplasm, accelerated. EV formation can occur when the cellular membrane closes a part of itself so that a new particle is formed. This is similar to what happens during cell division, but in the case of EV formation, the new particle does not contain all the cellular parts needed to make a functional cell. On the other hand, vesicles can contain many kinds of proteins and other substances both in their lumen and within their membrane. [56, 28] In the case of liposomes, the composition is well known and the size can also be controlled because they are synthetically produced, unlike extracellular vesicles. This control makes liposomes be significantly better suited than EVs for drug delivery and release applications as more homogeneous drug carriers lead to a more defined stimulus-response and the ability to use modified phospholipids and other synthetic components opens the possibility to use entirely different kinds of release mechanisms compared to EVs. [25, 84, 89, 76] In addition to liposomes, phospholipids can also be used to produce other lipid nanoparticles (LNPs), which is a more general term than vesicles. These particles, like liposomes, are composed of phospholipids and can be used for payload delivery; for example, in vaccines. However, because their internal structures can be significantly less ordered (they do not even have to contain bilayers), they are outside the focus of this thesis. [135]

1.2.1. Structure of liposomes

To clarify how this tunability arises, a brief review of the molecular basis of liposome assembly is provided. The primary structural units of cellular and vesicular membranes are phospholipids. These are biological molecules with a phosphate-containing polar, hydrophilic head group and two non-polar, hydrophobic hydrocarbon chains. This amphiphilic structure allows phospholipids to be soluble in both hydrophobic and hydrophilic environments and they can also act as surfactants, spontaneously forming an interface layer between such environments. The head group determines the charge of a phospholipid molecule, and in nature, it

often comes in the form of phosphatidic acid (PA), phosphatidylcholine (PC), phosphatidylethanolamine (PE), or phosphatidylserine (PS) among others. In addition, synthetic phospholipids can contain head groups from a virtually unlimited set of structures. Similarly, fatty acid tail group (acyl chain) lengths can vary, with the most common size being 16 to 18 carbons in biological membranes. [19, chap. 12] Commercial catalogs list options from single digits to at least 24 carbon atom chain lengths. [162, 30]

The acyl chain length also has an effect on the membrane phase transition temperatures. Below a certain temperature, the phospholipids in the vesicle membrane are packed together and are not diffusing around; this is called the gel phase. Membranes in this state are more rigid/less fluid and relatively slow to respond to disturbances. [19, chap. 12] Above this temperature, the phospholipids are constantly moving in the membrane and there is space between the tail groups. This is called the liquid crystalline phase, which is leaky because substances (such as drugs in the case of drug delivery and release) can diffuse through the soft membrane. However, the transition between the two phases is even leakier than the liquid crystalline phase. This transition temperature is called the gel to liquid crystal phase transition temperature (T_m) and longer chains lead to a higher T_m. ([19, chap. 12], [100, 116])

The saturation level of the fatty acids also affects membrane fluidity and phase behavior. For example, 18:0 PC (1,2-distearoyl-sn-glycero-3-phosphocholine, DSPC; here "18:0" denotes an acyl chain with 18 carbons and 0 double bonds) has a T_m of 55 °Cwhile that of 18:1 PC (1,2-dioleoyl-sn-glycero-3-phosphocholine, DOPC), with one double bond in the chain, is -17 °C. This is because an unsaturated bond in the acyl chain introduces a kink and consequently increases membrane fluidity as the phospholipids are forced slightly further away from each other, decreasing the attractive forces between them. ([19, chap. 12], [110, 59, 3])

Figure 2 shows two examples of common phospholipids and two examples of membrane stabilizing agents. Dipalmitoylphosphatidylglycerol (DPPG) (Figure 2a) is a negatively charged phospholipid with an acyl chain length of 16 carbon atoms and a T_m of 41 °C. The charge helps prevent liposome fusion [134]. 1-Palmitoyl-2-oleoyl-sn-glycero-3-phosphocholine (POPC) (Figure 2b) is a neutral, asymmetric, monounsaturated (containing one double bond in the lipid tail) phospholipid with chain lengths of 16 and 18 carbon atoms (one chain is longer than the other) and a T_m of -2 °C. [3, 26] Cholesterol, which, as a sterol, is a lipid based on a steroid nucleus (Figure 2c), acts as a stabilizer in the membrane by making it more flexible when the temperature is below T_m and more rigid when the temperature is above T_m, effectively buffering the fluidity of the membrane. ([19, chap. 12], [70]) Synperonic F108 (Figure 2d) is a block copolymer that only partially intercalates with the membrane and most of the molecule is exposed to the opposite sides of the membrane, sterically blocking other objects from touching the membrane. This is another way to stabilize liposomes because it reduces disturbances of the membrane structure. [125]

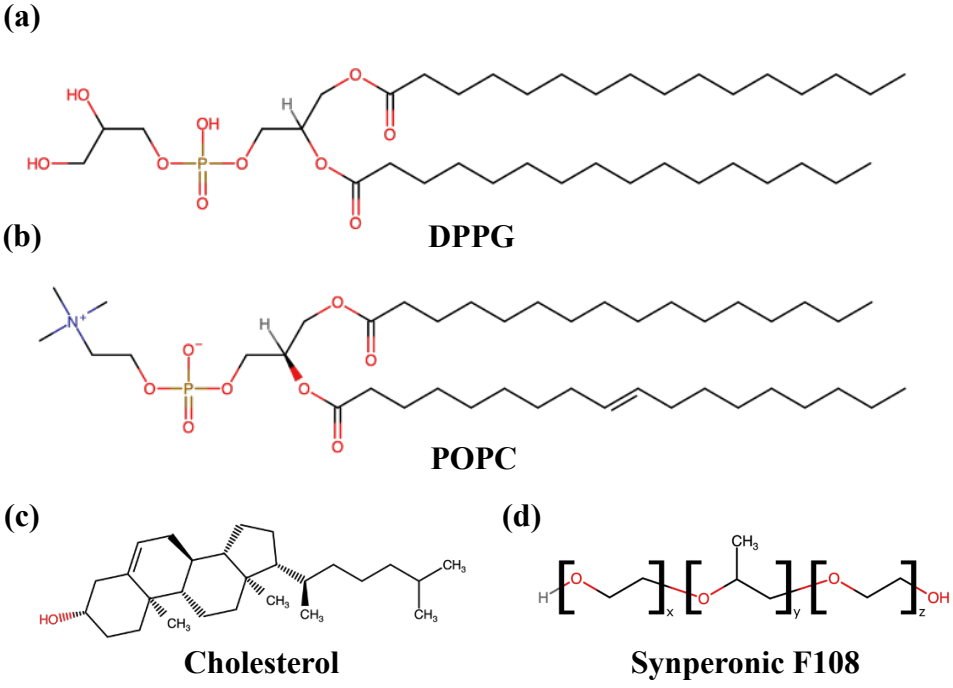

Figure 2: Examples of phospholipids and membrane stabilizers. (a) Dipalmitoylphosphatidylglycerol (DPPG) (charged) and (b) 1-palmitoyl-2-oleoyl-sn-glycero-3-phosphocholine (POPC) (neutral) as examples of phospholipids. (c) Cholesterol and (d) Synperonic F108 as examples of natural and synthetic membrane stabilizers, respectively. The letters x, y, and z indicate that the blocks in the brackets are repeated x, y, and z number of times in the polymer.

1.2.2. Liposome production methods

Together, the structural and compositional choices determine which fabrication routes are feasible and how stable the resulting vesicles will be, motivating a brief overview of liposome production methods. For example, in the case of thin film hydration (TFH) (also known as the Bangham method) (Figure 3a), which was the first widely used laboratory-scale liposome production technology, a thin (multilamellar) film of phospholipids is formed by depositing phospholipids in an organic solvent on the inner surface of a container and evaporating the solvent. The film is then hydrated with an aqueous solution under agitation, causing the phospholipids to self-assemble into bilayers that peel off and close into spherical vesicles, forming heterogeneous multilamellar liposomes. [13, 83]

In the case of solvent injection (commonly referred to as ethanol injection), a solution of phospholipids in a water-miscible solvent, such as ethanol, is injected into a larger mass of water while stirring, and the original phospholipid solvent is subsequently removed by evaporation or dialysis. It is a technique for efficient solvent exchange, where phospholipids dissolved in a non-aqueous solvent are suddenly exposed to an aqueous environment and self-assemble into liposomes as a result (Figure 3b). [16, 145, 83]

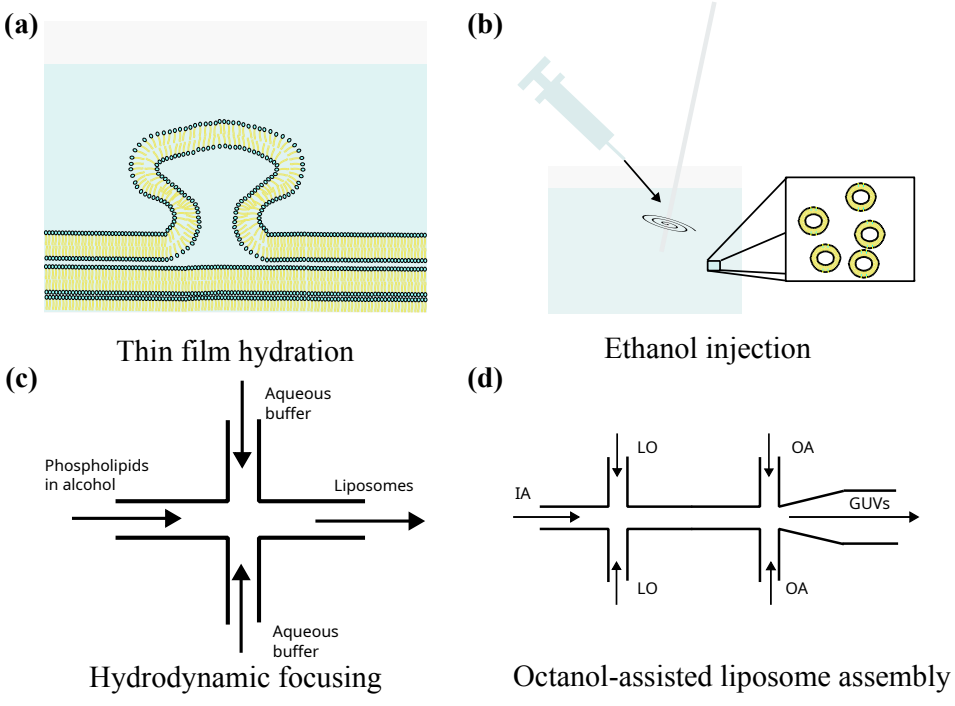

Figure 3: Examples of liposome production methods. Different ways to produce liposomes. (a) Thin film hydration (TFH). (b) Ethanol injection. (c) Hydrodynamic focusing (HDF). (d) Octanol-assisted liposome assembly (OLA) method for GUV production. IA – inner aqueous phase, LO – lipid-oil, OA – outer aqueous phase.

The most obvious way to load payload into the lumens of these liposomes is by dissolving it in the bulk aqueous liquid in the case of solvent injection or the hydration buffer in the case of TFH. The payload will be encapsulated within the liposome lumens as the liposomes form in the buffer that contains the payload. This is not a very efficient way of loading in that a large amount of the payload is necessarily left non-encapsulated. ([19, chap. 12], [16]) If there is a need to incorporate some material into the membrane, then it must be first mixed with the phospholipids in solution and dried to form the thin film that is subsequently hydrated in the TFH method. [19, chap. 12]

To gain more control over the size distribution of the liposomes produced using the solvent exchange approach, it is possible to use a microfluidic hydrodynamic focusing (HDF) approach (Figure 3c). In this case, an alcohol-based solution of dissolved phospholipids is jetted into a stream of water-based solvent inside of a microfluidic chip. This leads to a more homogeneous size distribution compared to the ethanol injection method that can be influenced by adjusting the flow rate ratio of alcohol to water. [164]

It should be noted that it is still possible to get relatively uniform liposome size distributions also with TFH and ethanol injection by incorporating post-formation processing steps, such as extrusion and sonication. In the case of extrusion, the liposomes are passed through a membrane filter with a selected pore size one or more times in order to force larger liposomes to reform towards the size dictated by the pores. [105, 20] In the case of sonication, the liposomes are exposed to ultrasound in order to reduce their size. This also tends to reduce the polydispersity of the liposome solution. [152, 131]

All of the above mentioned production approaches are based on the self-assembly of phospholipids into liposomes, relying on the natural tendency of phospholipids to form spherical bilayers. [19, chap. 12] In other words, these approaches are stochastic and yield highly heterogeneous liposomes. One higher-control method for liposome production using microfluidics is based on creating a water-in-oil-in-water emulsion and is called octanol-assisted liposome assembly (OLA). This method could be viewed as the microfluidic equivalent of the droplet transfer method from Yanagisawa et al. [155], where droplets of inner aqueous media fall through a phospholipid containing oil phase into a bulk outer aqueous medium. Figure 3d shows an OLA microfluidic chip with three inputs, one oil-phase and two water-phase liquids that are combined to yield GUVs. This approach, like the droplet transfer method, makes it possible to separately control the composition of inner and outer aqueous liquids at production time and to load arbitrary (including very large) payloads into liposomes. On the other hand, these approaches can only produce GUVs. [31, 156, 155]

Table 1 provides a non-exhaustive overview of common liposome production methods. While Figure 3 introduced ethanol injection, HDF and OLA, the table also includes electroformation, solvent inversion, reverse-phase evaporation and detergent removal methods. These examples highlight the overall diversity of

strategies available when selecting an appropriate liposome production method. Among these, the OLA and HDF methods are also used in this thesis.

Table 1: Liposome production methods.

Method	Working principle	Assembly regime
Thin film hydration (TFH) [83]	Hydration of dried bilayers	Stochastic self-assembly
Solvent/Ethanol injection [83]	Simple mixing	Stochastic self-assembly
Solvent inversion [23]	Diffusion driven solvent exchange	Stochastic self-assembly
Hydrodynamic focusing (HDF) [164]	Microfluidic mixing	Controlled self-assembly
Octanol-assisted liposome assembly (OLA) [156]	Microfluidic assembly	Template-guided assembly
Electroformation [118]	Field-driven hydration of bilayers into GUVs	Field-assisted assembly
Reverse phase evaporation [7]	Emulsification followed by solvent removal	Emulsion mediated assembly
Detergent removal [7]	Lipids are solubilized in detergent, then purified to form bilayers	Micelle to bilayer transition
Droplet transfer [155]	Lipids are solubilized in a light oil phase, then water droplets falling through that phase form first micelles, then liposomes	Micelle to bilayer transition

Bold methods are used in this thesis.

1.2.3. Applications and properties

Because liposomes are composed of phospholipid bilayers, which closely resemble natural biological membranes, they can exhibit relatively low immunogenicity, especially when surface-modified with materials like polyethylene glycol (PEG) (PEGylated). This allows them to circulate in the bloodstream with minimal recognition by the immune system. [89, 142, 136] In addition to their stealth characteristics, liposomes have potential to be used for drug delivery to the central nervous system as they can be engineered to cross the blood–brain barrier by the use of cationic phospholipids in their composition. This is attributable to

their similarity to EVs, which are naturally employed by the body for intercellular communication and transport of materials across biological barriers. [89, 142]

Liposomes are also very versatile for the fact that they can encapsulate a wide range of payloads: hydrophilic substances and particles can be loaded into the lumen, whereas hydrophobic payloads can be embedded within the membrane. The lipid bilayer provides a protective barrier that prevents the payload from interacting with the environment. [14, 89, 143]

Liposomes can be made fusogenic by carefully selecting the phospholipid composition (neutral, cationic and aromatic group modified phospholipids) so that the membrane tends to merge with the normally slightly negatively charged cell membranes. The positive head group charge makes the liposomes be attracted to cell membranes. The aromatically modified head groups interacting with the positively charged phospholipids make the liposome membrane slightly unstable, making it prone to merging with cell membranes. [29, 71] These liposomes could be used to incorporate particles or transmembrane proteins into cell membranes as well as to transfer hydrophilic substances directly into the cytoplasm of cells. [29, 71, 87, 113].

Due to these characteristics, liposomes have been used in the clinical practice of drug delivery for decades to regulate drug release rate and for targeted delivery; for example, in Doxil and AmBisome. [14, 89, 128]. However, these clinically used solutions all have passive release control mechanisms, there is no active externally controlled trigger, such as light, ultrasound or magnetic field, causing the payload release. For the payload release rate, the composition of the bilayer can be tuned to allow for slow spontaneous payload leakage, or the membrane can be disturbed using other methods, such as magnetic fields in the case of magnetoliposomes, for actively controlled payload release. [6]

Another application of liposomes is using them as model systems in research. For example, GUVs have been used to investigate the effect of various factors on membrane properties, including the influence of peptides, photoacoustic waves and magnetic nanoparticles. They have also been used as cell models. [5, 133, 109, 75, 38]

1.2.4. Liposomes for controlled drug release

An advantage of active control of payload release over passive control is that off-target interactions can be reduced by restricting the area of payload release to only the areas of interest, thus increasing the TI, regardless of any microenvironment similarities in different areas of the body. One promising way to achieve this kind of effect is using special kind of liposomes in which superparamagnetic nanoparticles, such as iron oxide, barium-hexaferrite, or other magnetizable materials, are incorporated into or associated with the membrane (see a superparamagnetic iron oxide nanoparticle (SPION)-loaded liposome in Figure 4a). These are commonly referred to as magnetic liposomes or magnetoliposomes. The particles should

be small enough to consist of only a single magnetic domain to make sure that they are superparamagnetic so that they do not stay magnetized in the absence of external fields.

Usually, the magnetic particles are associated with the membrane by loading them between the phospholipid bilayer or attaching them to the surface using charge or via anchor molecules. Magnetic liposomes can become temporarily permeable when an external oscillating magnetic field is applied to them (Figure 4b). In the case of a low frequency (~ 50 Hz) oscillating magnetic field, the mechanism appears to be a physical membrane disturbance, as depicted in the figure. With high frequency (~ 100 kHz) magnetic fields, the mechanism is based on the heat generated from Neel relaxation causing a phase transition boundary to appear in the membrane, which creates space for material to move through the bilayer. This externally triggered permeability opens up the potential for magnetic liposomes to be used for drug delivery and release applications. [113, 89, 143, 94]

It deserves a mention that, while any liposome carrying magnetic particles may be called a magnetic liposome, if the particles are not attached to the membrane, the effect that external magnetic fields have on the permeability of the membrane is much smaller than when they are associated with the bilayer. [47, 89]

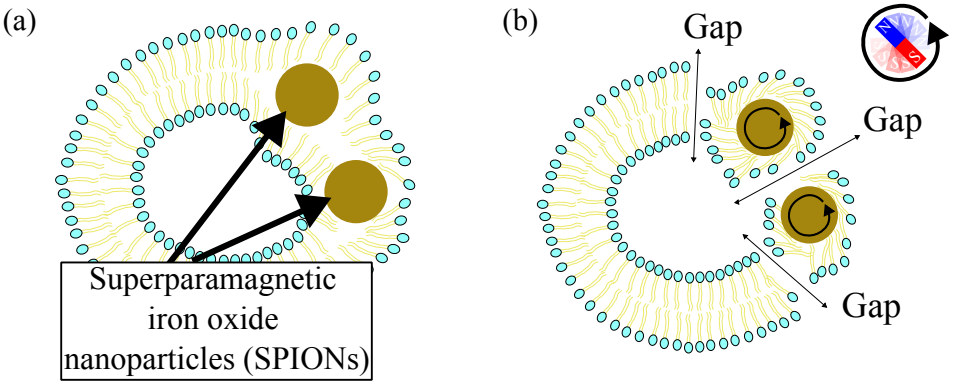

Figure 4: Magnetoliposomes. (a) Magnetoliposome at rest. (b) Permeabilization through gap formation under an oscillating magnetic field.

The use of magnetic liposomes in the development of drug delivery and controlled drug release systems has previously been reported in the literature. [113, 89] For example, Guo et al. [51] used magnetic liposomes loaded with doxorubicin and coated with methotrexate to target cells with folate receptors on their surfaces. These liposomes were shown to increase the spatial precision of drug delivery by using a combination of magnetic field and laser light based targeting. Y. Liu et al. [81] used magnetic particles embedded in liposomes to direct them into the target area and as contrast agents to be able to observe the migration of the liposomal carriers using a magnetic resonance imaging (MRI) machine. Nappini et al. [95] found that a 5.2 kHz magnetic field applied to magnetic liposomes will cause them

to switch from the gel phase to the liquid crystal phase after about 5 to 8 h. This renders the liposomes permeable and the payload (drug) is then able to leak out of the carriers. J. F. Liu et al. [80] demonstrated the possibility of remote-controlled localized triggering of payload release from magnetic liposomes. In that case, the mechanism involves the use of a static gating field and a dynamic triggering magnetic field to cause the particles in drug-carrying liposomes to release their payloads only in specific areas in space.

1.3. Microfluidics

As mentioned above (Table 1), some of the ways to make liposomes involve the use of microfluidics. This is a field that manipulates liquids using chips with channel diameters on the order of micrometers. At this scale, surface tension and diffusion play a significant role in determining the behavior of liquids. It offers versatile platforms for a wide array of applications where small volumes and high precision are required. They are employed as mixing devices and reaction chambers for both chemical synthesis and biological processes, such as polymerase chain reaction (PCR). These systems enable the creation of liposomes, generation and manipulation of droplets (emulsions), and efficient mixing of liquids. For instance, microfluidic droplet generators can efficiently produce thousands of individual reaction compartments, which serve as miniature "vessels" for high-throughput biochemical reactions. Such high throughput methods make it possible to investigate the variability among individual cells, including antibiotic susceptibility testing, metabolic pathway analysis, and evolutionary studies by studying growth heterogeneity. Similarly, microfluidic techniques are widely employed for liposome and LNP synthesis, allowing controlled size distribution and encapsulation efficiency. [164, 15, 156, 121, 98, 97, 161]

Microfluidic devices can also serve as growth chambers for bacteria and mammalian cells, organ-on-chip systems, and nanomaterial (including nanogel) synthesis platforms. Growth chambers typically consist of microfabricated compartments in which cells can be cultured under controlled conditions while nutrients and signaling molecules are continuously supplied through microchannels. These systems facilitate studies of chemical effects and concentration-dependent responses in cell populations. [50, 124] Furthermore, single-cell analysis can be achieved by isolating individual cells within microchambers [149]. Related applications include assessing blood cell deformability using microfluidic constriction channels [37]. Organ-on-chip systems represent another significant application of microfluidics. These devices integrate living cells within environments that mimic tissue architecture and physiological conditions. They incorporate perfusion channels for nutrient delivery and waste removal, and can include mechanical actuation to simulate mechanical strain to provide a more physiologically relevant model for drug testing and disease modeling. [61, 63, 112]

A slightly different type of application for microfluidics is the use of various sensors. For example, most pregnancy tests are lateral flow devices where the liquid is introduced at the inlet and travels to the detection zone and can technically be considered to be microfluidic devices. In this case, there are technically no microchannels, but rather the liquids travel along a paper strip. [157, 4, 119] Microfluidics has also been used to develop actuators and touch sensors for soft robotics applications. [146, 58]

1.3.1. Pressure and flow control

Microfluidic devices work on the basis of liquid flow through microchannels. The Navier–Stokes equations describe the flow of incompressible Newtonian liquids:

$$\rho(\frac{\partial u}{\partial t} + u \cdot \nabla u) = -\nabla p + \eta \nabla^2 u + f, \tag{1.1}$$

where ρ is the density of the liquid, u is the flow velocity field, p is the pressure, η is the viscosity of the fluid, f represents an external body force per unit volume, and $\nabla \cdot u = 0$. [126] Because viscous forces generally outweigh inertial ones in microchannels, the equation can be simplified to the Stokes flow regime [126, 74]:

$$-\nabla p + \eta \nabla^2 u + f = 0. \tag{1.2}$$

Therefore, the immediate cause of liquid flow is the pressure gradient. This is true even for a simple flow controller, such as a syringe pump. The plunger motion sets a volumetric rate upstream, but the flow in the chip still arises from the pressure that hydraulic resistance and compliance create in the fluid path. [159, 77]

To work with microfluidics, it is important to have good control over the flow rates of the liquids in the chip. The two main ways to control the flow of liquids in a microfluidic chip are flow control (using a device such as a syringe pump) and pressure control (using a pressure controller). [73, 77, 159]

In volumetric flow-controlled systems, such as syringe pumps, a computer-controlled piston moves the plunger at a defined speed to impose a programmed volumetric flow rate. Because the pump acts like a current source, the inlet pressure needed to sustain the flow rate depends on the compliance of the syringe, tubing, and chip walls. This compliance leads to slower settling and rate-dependent transients. [65] Pressure-based control has a much quicker response time because these controllers actively change the pressure that moves the liquid through the microfluidic system. Pressure changes in the system propagate at the speed of sound. It can also be more stable than flow control because pressure controllers avoid the small mechanical irregularities seen in the syringe-pump systems, for example, jittering stemming from the difference between the dynamic and static friction of the plunger. These fluctuations can cause problems in sensitive applications, such as flow cytometry or homogeneous droplet/liposome generation. [164, 57, 77]

The most common way to automatically maintain stable control over physical parameters like pressure is by using a proportional-integral-differential (PID) algorithm, which is a feedback-based loop control algorithm that works by continuously calculating and summing three error value-based mathematical terms (Equation (1.3)):

$$m(t) = K_{\mathrm{p}}\varepsilon(t) + K_{\mathrm{i}}\int_0^t \varepsilon(\tau)d\tau + K_{\mathrm{d}}\frac{d\varepsilon(t)}{dt}, \tag{1.3}$$

where $m(t)$ denotes the value of the manipulated (controlled) output variable. K_{p}, K_{i}, and K_{d} are the proportional, integral, and derivative gains, respectively. These gains are controller parameters that are optimized per application. [21] The error value $\varepsilon(t)$ denotes the deviation of the controlled parameter (such as pressure) from the setpoint (reference value) at time t. The integration variable τ represents past time values over the interval $[0,t]$. ([9, chap. 10]; [21])

The proportional term in Equation (1.3) reacts directly to the error value and increasing it can lead to a faster response, but it can also lead to overshooting the target and instability if it is too large. The derivative term is meant to dampen oscillations and reduce overshooting. Finally, the integral term is meant to eliminate long term errors and increasing the K_{i} can improve the response speed; but again, too high values can lead to instability. Finally, the derivative term is used to predict future errors based on the rate of change of the measured error value. It improves stability in cases where the controlled parameter has a lot of inertia and the controlled (process) variable changes slowly. [9, 21]

1.3.2. Pressure and flow control device types

In practice, the advantages of pressure- versus flow-based control are realized only if the hardware delivers the required performance characteristics, including response time, stability, and chemical compatibility. Practical factors such as cost and ease of use must also be considered.

Syringe pumps are widely used flow controllers for small-scale microfluidics. They are inexpensive and simple to deploy. However, they can exhibit flow-rate / pressure oscillations due to motor steps and mechanics and sample wastage from upstream dead volumes (syringe barrel, fittings, tubing). [55, 10, 18]

Peristaltic pumps are another relatively affordable flow control solution. Compared to syringe pumps, they offer the ability to dispense virtually unlimited amounts of liquid together with the possibility to recirculate the same liquid in a closed system. On the other hand, they also come with the drawbacks of higher flow pulsation, typically not being able to produce very low flow rates, as well as overall lower dispensing accuracy. [18, 45]

Piezoelectric pumps are small self-contained flow controller devices that can also be used to drive liquids. They offer quicker response times compared to syringe pumps and can also be used for continuous pumping, like peristaltic pumps.

One drawback is that they are less resistant to harsh chemicals, like organic solvents, because the liquid flows through the pump. Also, they can only pump relatively low viscosity fluids and have significant backflow. [154]

Pressure controllers/pumps are typically (but not in every example) the most advanced and also the most costly solutions for driving the flow of liquids in microfluidic systems. They offer the most stable operation and the fastest response times. They are also the best solution when very low flow rates are desired because control over low flow rates requires high precision and stability. [106, 159]

The simplest way to achieve pressure control is to apply hydrostatic pressure by placing the reservoir higher than the chip, allowing gravity to pull the liquid into the chip. [24, 96] The more common way to use pressure in microfluidic experiments is by using a pressure pump or controller. These systems create a pressure difference between the inlet and outlet containers of a microfluidic system. This means they cannot be used to continuously recirculate liquids in a closed-loop configuration as it is not possible to create a loop where one point is at the same time at the lowest and the highest pressure level (except the trivial solution of no flow). [104] However, unlike with syringe pumps, arbitrarily large reservoirs can be used with pressure controllers as the reservoir itself does not actuate the liquid. These solutions offer the fastest response times, since pressure is the fundamental driving parameter behind flow in microfluidic systems, as discussed in Section 1.3.1. With these controllers, it is possible to achieve pulseless flow and they can have near-zero dead volume as air can push all the liquid out of the tubes and through the microfluiodic chip. [73]

The other drawback of the pressure control approach compared to flow control systems (like syringe and peristaltic pumps), is the possibility of backflow if the relative input pressures fluctuate.[160]. Mitigations for this include directional valves and careful planning of the relative pressures and their changes in an experiment. For example, it is possible to use a vacuum as the primary driving factor and adjust the relative flow rates of the different input liquids by applying significantly weaker positive pressures to the input channels. [62, 160]

1.3.3. Practical considerations for reliable microfluidic operation

In addition to the constraints introduced by different flow and pressure controllers, achieving the correct operating regime in microfluidic chips is a non-trivial task and may require maintaining laminar streams for controlled mixing or, conversely, inducing local instabilities or shear to promote droplet breakup and vesicle formation. [156, 164]

Generally, it is important to remove all air from a microfluidic system at the beginning of an experiment. Due to surface tension, bubbles tend to adhere to channel walls. This issue is especially pronounced with chips that are made of hydrophobic materials, such as polydimethylsiloxane (PDMS), where water does

not wet the inner surface of the chip as readily as it would with a hydrophilic material. [156]

Another challenge is related to the sorption, wettability, and solvent compatibility of materials. PDMS is widely used because it is optically clear and convenient, but it absorbs and adsorbs hydrophobic small molecules and can skew concentrations and cause time-dependent leaching. It also swells in many organic solvents. Quantitative studies show losses exceeding 90% for high partition coefficient compounds and slower washout due to bulk absorption compared to thermoplastics like cyclic olefin copolymer. Mitigations include coatings, careful solvent pairing, and switching to glass or thermoplastics if chemical compatibility and minimal sorption are needed. [139, 147, 49]

Partly related to sorption are the phenomena of biofouling and clogging. Cell, colloid, or protein suspensions can aggregate and clog microchannels, degrading chip performance and reducing experimental reproducibility. Reviews also highlight sieving and adhesion as common mechanisms for this phenomenon. Geometry optimization as well as emerging strategies like microbubble streaming can be employed to reduce arch formation (bridging) and cluster buildup. For adsorption and adhesion, the main alleviation strategies are careful selection of chip materials and microchannel coating. [33, 12, 139, 49]

In some applications, such as PCR chambers, it is important to have precise and uniform control of temperature. Rapid heat transfer and large surface-to-volume ratios inherent to microscale systems make uniform temperature control challenging. Proposed solutions include specially designed channel topologies, PID controllers with both heating and cooling elements, as well as photothermal heating approaches. [153, 122, 64] Open or partially open systems, as well as semi-permeable chip materials, such as PDMS enable evaporation that can change concentrations and disrupt reactions. Recent reviews and designs propose closed-loop heating, integrated sensing, diffusion-limited layouts and even the use of mineral oil in the uncured PDMS mixture to suppress evaporation during thermal cycling. [122, 49, 64]

Despite these challenges, microfluidics enables precise fluid manipulation, fast reactions, minimal reagent consumption, and integration of complex workflows on chip. In particular, droplet microfluidics offers compartmentalization for single-cell analysis, high-throughput screening, and tunable material synthesis, while microfluidic nanoparticle formulation improves batch-to-batch reproducibility and control over size and loading. [147, 98, 149, 37, 31]

1.4. Dose-response and heterogeneity in microcompartment assays

Liposomes and droplets exhibit comparable appearances in microscopy images, which allows them to be analyzed with similar computational methods. High-throughput droplet (emulsion) studies already provide a substantial foundation in

this regard, particularly in work focused on bacterial growth and antibiotic susceptibility. In such experiments, dilute bacterial suspensions are encapsulated in water-in-oil droplets so that, according to Poisson statistics, most droplets contain either no cell or a single cell, typically at average loading values of 0.1 to 0.3 cells per droplet. This configuration enables single-cell level measurements. Even with identical inputs, outcomes vary across compartments in ways that are not visible in bulk measurements. Because liposomes and microdroplets share key morphological features relevant for image processing, the same analytical principles can be transferred between the two systems. This section introduces the basic terminology and summary measures used to describe such variability. These definitions complete the conceptual groundwork for the research statement and objectives that follow. To anchor the terminology in a concrete setting, single-cell bacterial assays in droplets provide parallel readouts that reveal meaningful variation across nominally identical compartments, motivating robust analytical methods to quantify and model these differences. [149, 97, 161, 93]

For antibiotic susceptibility testing in particular, droplet-based approaches enable high-throughput analysis where potency is commonly analyzed using a concentration-viability plot (antibiotic concentration on the horizontal axis, often log-scaled, and bacterial cell viability on the vertical axis). The resulting viability (dose-response) curve is typically sigmoidal (S-shaped). [127] The concentration yielding 50% viability is the inhibitory concentration $(\mathrm{IC})_{50}$ when testing a single strain of bacteria, or minimum inhibitory concentration $(\mathrm{MIC})_{50}$ when testing a population of different strains of bacteria.

The Gompertz model is a sigmoidal mathematical function, discovered by Benjamin Gompertz in 1825 to model human life expectancy [111], that is widely used to model growth curves and for survival analysis, as well as other phenomena, such as the decay of the adoption rate of technological products. It captures the lag phase, exponential growth, and stationary phase of bacterial populations via an unusual double exponent equation[165]:

$$y(t) = A \cdot \exp[-\exp(\frac{\mu e}{A}(\lambda - t) + 1)], \tag{1.4}$$

where $y(t)$ is population size at time t, A is the maximum population size (asymptote), μ is the maximum growth rate and λ is the lag time before exponential growth and e is Euler's number. By fitting bacterial growth data to the Gompertz equation, it is possible to estimate how substances, such as antibiotics, affect their growth. By analyzing the curve's shape and inflection point, the MIC of an antibiotic and related metrics can be determined.[165, 138]

The Gompertz model is not necessarily the most accurate representation of the viability curve, therefore, other s-curve functions are also used, for example Equation (1.5):

$$y(c) = \frac{1}{1 + (\frac{c}{c_{\text{scale}}})^{\alpha} + a_1(\frac{c}{c_{\text{scale}}})^{2\alpha}}, \tag{1.5}$$

where c is the antibiotic concentration and c_{scale}, α, and a_1 are parameters that need to be fitted using the least-squares method. [123]

Instead of reporting a single MIC value, modern approaches model MIC as a distribution across a population or replicate measurements. This accounts for variability and uncertainty. A probability density function then shows how likely different MIC values are. For example, a narrow peak near 28 ng/mL, the red graph in Figure 5, indicates that most cells are inhibited at that particular concentration, whereas the broad distribution, in blue, reveals heterogeneity in resistance. [90, 150]

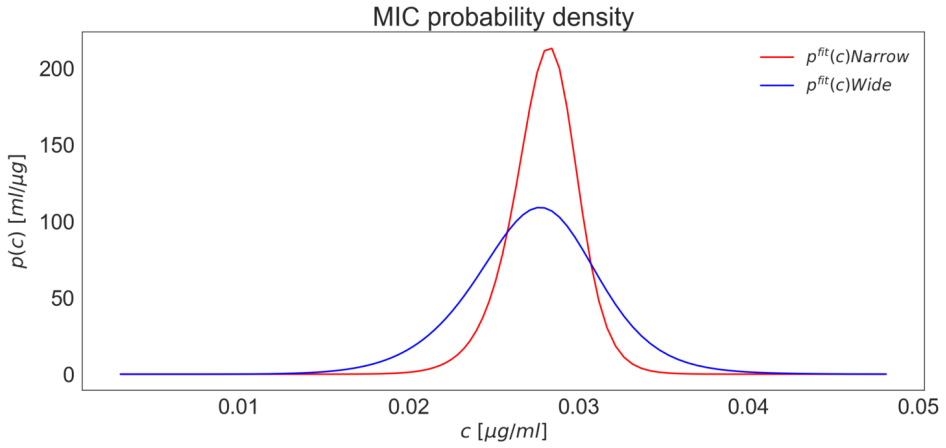

Figure 5: MIC probability density. Example of a narrow and a wider probability density as a function of concentration ($p(c)$) as calculated from a fitted cell viability curve, plot of minimum inhibitory concentration (MIC) values across bacterial strains. In this figure, MIC denotes MIC_{50} (the concentration inhibiting 50% of isolates).

1.5. Research statement and objectives

While high frequency magnetic field induced permeabilization of liposomes has been extensively studied, the low frequency approach remains comparatively underexplored. Published work on magnetoliposomes has not yet advanced the technology toward clinical translation and none of the reported systems have reached clinical trials. Consequently, while the technology readiness level (TRL) of magnetoliposomes remains below 6 (stage 1 clinical trials), magnetic liposomes actuated by very low frequency magnetic fields are still only at TRL 1. The work in this thesis focuses on the preliminary steps needed to explore this gap by developing liposomes suitable for systematic experimentation with the goal of advancing magnetic liposomes actuated by very low frequency fields from TRL 1 (observation of low frequency magnetic field based permeabilization of membranes) toward levels 2 or 3 (proof of concept for remote controlled and localized permeabilization of membranes). At this early stage, the focus is not on producing

clinically injectable carriers, as is the case with high frequency magnetic fields, but on developing model systems that make the underlying release mechanisms experimentally accessible. In this context, it is necessary to develop closed compartments based on phospholipid bilayers to achieve this goal. [8]

This thesis aims to increase the accessibility of reproducible microfluidic and analytical methods for liposome fabrication and characterization, and to determine quantitative baselines for stability and passive leakage that will enable future model-based *in vitro* studies of localized payload release.

Achieving this goal requires overcoming key challenges, including creating a more financially attainable pressure source that features high output precision and stability, for microfluidic experiments, and establishing robust quantitative methods to assess the cargo loading efficiency and release dynamics of liposomes. The work addresses these challenges by designing and testing a pressure regulator device and contributing advanced image analysis tools, methodologies, and model particles to enable the future development of magnetically responsive liposomes for localized drug delivery.

Paper I: Development of an affordable microfluidic method to produce GUVs, that could be characterized under an optical microscope, with the aim of creating a model system for phospholipid membrane characterization and *in vitro* payload release studies. Demonstration of the encapsulation of various payloads into GUVs. Determination of the stability of the GUVs and their spontaneous payload release characteristics.

Paper II: Development of an affordable, stable, and precise pressure controller for stable microfluidic applications. Demonstration of the usefulness of the device by the production of SUVs using a HDF method.

Paper III: Development of new software requiring no programming expertise for post-image analysis of particles in droplet experiments, along with methodological pipelines for preparatory analysis steps.

2. MATERIALS AND METHODS

In this work, liposomes of a wide range of sizes (from 100 nm SUVs to 100 μm GUVs) were produced and investigated. This necessitated the use of both optical and electron microscopy. The liposomes were produced using two microfluidic techniques, and their stability was characterized by counting the liposomes from microscopy images at different time points as well as by a calcein leakage assay. A software for bulk analysis of droplets and liposome microscopy images was also developed. This chapter is a brief overview of these methods.

2.1. Optical microscopy

In order to monitor the microfluidic production of GUVs, an optical microscope was used (Eclipse TS-100, Nikon Instruments Inc., USA). This was necessary because the channel width of less than 100 μm of the microfluidic chips renders direct observation of experiments without magnification impractical. In addition, the use of microscopes enabled video recording of the process because the spatial resolution of the camera would not have been sufficient without the magnification of a microscope. However, they are inherently unable to resolve details that are smaller than the half wavelength of light (assuming a numerical aperture of 1), which is about 200 nm for blue light (wavelengths from 400 nm to 500 nm), unless more advanced super-resolution systems are not used [141]. This is described by Abbe's formula $d = \frac{\lambda}{2\mathrm{NA}}$, where d is the minimum distance between two points that can still be resolved, λ is the wavelength, and NA is the numerical aperture. [1, 43]

In an optical microscope, the light from the sample is first collected by an objective lens that creates a magnified real (with converging light rays) image at an intermediate image plane inside the microscope. Then, an ocular (eyepiece) lens converts the real image into a virtual (with diverging light rays) one that can be captured by the human eye or a camera. The total magnification of the microscope is determined by the product of the magnifications of the two lenses. [1] In the case of an inverted microscope, the sample is placed on top of the objective and a series of mirrors is used to view it from below. The light that is observed comes through the sample from above and therefore this kind of microscope is used to view transmitted light. On the other hand, a confocal microscope uses a system to filter out light that is out of focus and allows imaging of different layers of a sample. [53, 102] This kind of microscopy was used to investigate GUVs with magnetic microparticles loaded inside them (Section 3.4.2).

In fluorescence microscopy, light of a shorter wavelength (excitation light) is used to excite fluorescent molecules within a sample. These molecules subsequently emit light of a longer wavelength (fluorescent emission), which is then collected by the objective lens for imaging. Optical filters placed into the optical

path between the sample and the detector are used to ensure that only the emitted light is detected and the excitation light filtered out. This technique is widely used in biological research to visualize specific materials and structures in a wide range of samples, including living cells. It also enables the selective labeling of specific cellular structures with fluorescent marker molecules, enabling precise visualization of their localization and dynamics within the cells. Figure 6 depicts what a typical fluorescence microscope looks like. The excitation light is usually produced by a separate lamp module, it passes through a filter box and the objective lens, and finally reaches the sample. The fluorescence light is then emitted by the sample, which then passes through the objective lens, filter box, and is then directed to the ocular lens by a mirror. [78, 36] In this thesis, fluorescence microscopy was used to investigate GUVs produced via OLA (Section 3.4).

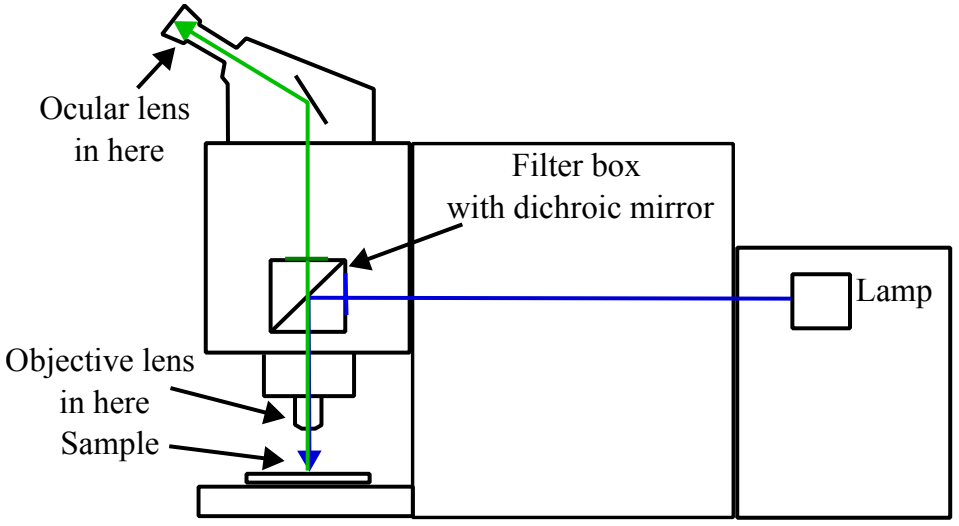

Figure 6: Fluorescence microscope. The excitation light comes from a specialized lamp, passes through a filter box (and the objective lens) and reaches the sample. The fluorescence light is emitted from the sample, passes through the filter box and reaches the ocular lens.

2.2. Electron microscopy

Since the resolution of basic optical microscopy is practically limited to the micrometer scale, other imaging methods, such as electron microscopy (EM) techniques, are needed to resolve structural details of the objects that are smaller than that, such as ~ 100 nm sized liposomes studied in this work. One of such techniques, transmission electron microscopy (TEM), generates high-resolution images by transmitting an accelerated and focused electron beam through a thin specimen. Because the de Broglie wavelength of accelerated electrons (< 10 pm

at > 20 kV) is several orders of magnitude shorter than that of visible light, EM can achieve much higher spatial resolution than optical microscopy. [108, 34]

Figure 7 contains a schematic of how the image is formed in a TEM. The electrons are emitted from the cathode and pass through a series of lenses and apertures on the way to the sample and also from the sample to the camera, which can be a phosphorous screen that is photographed or a charge coupled device (CCD) camera. [40]

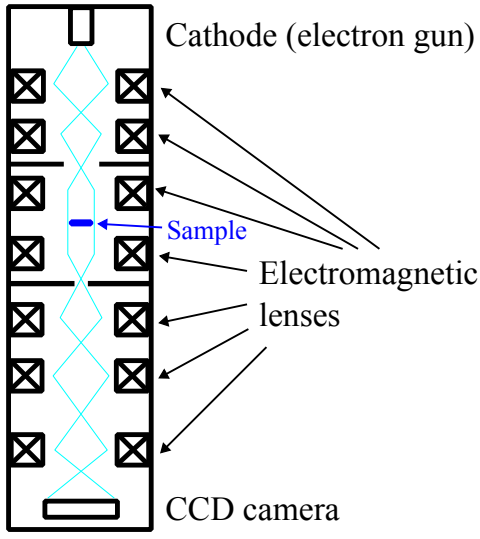

Figure 7: Transmission electron microscopy (TEM). The electrons are emitted from the cathode and pass through a series of electromagnetic lenses and apertures on the way to the sample and from the sample to the charge coupled device (CCD) camera that is placed on the bottom of the vacuum column.

The contrast of the resulting image arises from the variation in electron transmission, which depends on sample thickness and composition. To enable imaging, the specimen is mounted on a support grid, which is typically a copper mesh coated with a thin carbon film. The grid provides mechanical support while allowing electrons to pass through the sample regions.

For imaging liposomes with TEM, additional preparation is required because liposomes lack inherent electron density. They must be immobilized on the TEM grid and stained with electron-dense agents to enhance contrast. The staining might also help liposomes to maintain their shape to some extent during imaging so that their morphology can be resolved. [117]

In this work, negative staining with uranyl acetate was used to prepare SUV samples for imaging. A 5 μL droplet of suspended liposomes was pipetted on a formvar–carbon coated TEM grid made of copper and incubated for 5 min. The sample was then stained using a 2% aqueous uranyl acetate solution for 2 min. Finally, the sample was washed with a drop of deionized water and air dried.

The samples were imaged using a Tecnai G2 Spirit BioTwin (FEI, Hillsboro, OR, USA) transmission electron microscope configured at a 120 kV accelerating voltage and the images were captured using an Orius SC1000 CCD camera (Gatan Inc., Pleasanton, CA, USA). The imaging was performed in the Institute of Cellular and Molecular Biology, University of Tartu.

2.3. Dynamic light scattering (DLS)

Dynamic light scattering (DLS) was used to determine the size of liposomes with diameters in the nanometer range. This technique takes advantage of the fact that particles in a solution undergo Brownian motion, leading to time-dependent fluctuations in the intensity of scattered light. This phenomenon makes it so that the hydrodynamic radius of the particles can be calculated from the diffusion coefficient using the Stokes–Einstein equation (Equation (2.1)):

$$R_{\mathrm{H}} = \frac{k_{\mathrm{B}}T}{6\pi\eta D}, \tag{2.1}$$

where R_{H} is the hydrodynamic radius, k_{B} is the Boltzmann constant, T is the solution temperature, η is the viscosity of the solvent and D is the diffusion coefficient. [79, 92, 35] The size range of particles that a DLS instrument can detect is between about 1 nm and 1 μm [67, 68].

In a DLS instrument, the intensity of scattered light is analyzed through an autocorrelation function, which measures the similarity of the signal (autocorrelation) at two subsequent points separated by a delay time, τ. This is calculated according to Equation (2.2):

$$g^2(\tau) = \frac{\langle I(t)I(t+\tau)\rangle}{\langle I(t)\rangle^2}, \tag{2.2}$$

where $g^2(\tau)$ is the autocorrelation function at a particular delay time τ, and I is the intensity of a scattered light as a function of time. [41]

The autocorrelation of the scattered light drops over time depending on the size of the particles. Smaller particles move around faster and therefore the autocorrelation of the scattered light from those particles decays faster compared to that from larger particles. For polydisperse systems, the measured autocorrelation function represents a superposition of decays arising from particles with different diffusion coefficients. This decay is analyzed using cumulant analysis, which yields the average autocorrelation decay rate and higher-order cumulants describing the width of the decay-rate distribution. The mean diffusion coefficient obtained from the first cumulant, Γ, is then converted into a corresponding hydrodynamic particle size using Equation (2.1) from above. [41]

The quality of the correlation data strongly depends on the homogeneity of the sample. The polydispersity index (PDI) is used as a numerical parameter to gauge

the reliability of the measurement. It is calculated using PDI $= \frac{\mu_2}{\Gamma^2}$, where μ_2 is the variance of the fitted decay rates and Γ is the average autocorrelation decay rate. A low PDI indicates a narrow size distribution and reliable results, while a high PDI suggests the presence of multiple populations or aggregation, which complicates interpretation. When size distributions overlap, the peaks may merge, reducing the resolution and accuracy of the results. [41] Another way to express the PDI is as the square of the standard deviation (σ) of the particle diameter divided by the mean particle diameter (d) itself (PDI $= (\frac{\sigma}{d})^2$). [60]

All DLS measurements of HDF-produced liposome sizes and concentrations in this thesis were performed using a Zetasizer Ultra (Malvern Panalytical, Spectris PLC, London, UK). Samples were analyzed using a DTS0012 measurement cuvette. The ZS XPLORER software v3.31 (Malvern Panalytical) was configured to assume the dispersant to be water with a refractive index of 1.45 and absorption of 0.001. All the samples were prepared by diluting the sample itself in ultrapure water to reach the necessary sample volume with an appropriate dilution factor, which was typically 20x. The default concentration measurement protocol of the ZS Xplorer was used, performing three repetitions and averaging the results by the particle size bin values so that the concentration values measured for any given diameter were exported and manually added and divided by the number of measurements.

2.4. Octanol-assisted liposome assembly (OLA)

The octanol-assisted liposome assembly (OLA) approach uses a two-junction chip, the design of which is described in Yandrapalli et al. [156], to produce GUVs (100 nm diameter). This approach has the significant advantage of making it possible to load arbitrary water soluble payloads into the vesicles. The main downside of this method is that the liposomes produced contain some octanol inside their membranes, which may be problematic for some applications. In addition, these liposomes are relatively unstable due to their giant size.

A vacuum generator was connected via a polytetrafluoroethylene (PTFE) tube to a 50 mL centrifuge tube, which was in turn connected to the output channel of the microfluidic chip by another PTFE tube. Three input liquids were contained in 1.5 mL centrifuge tubes and connected to the chip via PTFE tubes (Figure 8). The input liquid tubes (inner aqueous phase (IA) – inner aqueous liquid, lipid-oil (LO) – phospholipids in octanol, outer aqueous phase (OA) – outer aqueous liquid) were manually raised and lowered to adjust the relative flow rates. This approach made use of gravity to adjust the input pressures.

During GUV production experiments, IA and OA reservoirs were filled with solutions containing 300 mM saccharides (sucrose and glucose from Merck , Germany) and 0.5% w/v Synperonic F108 (Croda International Plc, UK) dissolved in ultrapure water. The LO liquid was 5 mg/mL POPC (Avanti polar lipids, USA) dissolved in 1-octanol (Merck, Germany), which was stored at 4 °C and heated

to 60 °C for 30 min before each OLA experiment. As an exception, for the experiment where 3.2 μm diameter magnetic microparticles (COMPEL^{TM} Fluorescent Magnetic COOH, Microspheres, Glacial Blue (Bangs Laboratories, USA)) were loaded into the GUVs, the saccharide and Synperonic F108 concentrations in the IA and OA solutions were halved and 0.5 mg/mL of magnetic particles were added. For enhanced green fluorescent protein (eGFP) loading, 50 ng/μL of eGFP was added to the IA solution. The production and purification of eGFP from a bacterial expression system was performed according to the protocol in Reinsalu et al. [114]. For calcein loading and liposome counting experiments, 5 mM calcein was added to the IA solution, whereas for the calcein release experiments, the concentration was set to the self-quenching level of 60 mM.

In contrast to Yandrapalli et al. [156], who used an active pressure controller system to drive each of the input channels simultaneously, here a simplified setup with only a single Fluika VG350 vacuum generator (Dolomite Microfluidics, UK) was used to drive the liquids through the chip. An inverted optical microscope (Eclipse TS-100, Nikon Instruments Inc., USA) was used to monitor liposome production and the production process was captured by a high-speed camera (Huawei Technologies Co., Ltd., China).

To image GUVs after production, a fluorescence microscope (EVOS M5000, Thermo Fisher Scientific Inc., USA) was used for GUVs imaging and a confocal microscope (LSM710, Zeiss, Germany) was used to image the GUVs that contained magnetic microspheres.

As the correct operation of the OLA chip depends on the proper functionalization of the outlet channel walls, the chip was coated using polystyrene sulfonate (PSS, Merck, Germany) and polydiallyldimethylammonium chloride (PDADMAC, Merck, Germany) using the protocol from Yandrapalli et al. [156] to render it hydrophilic.

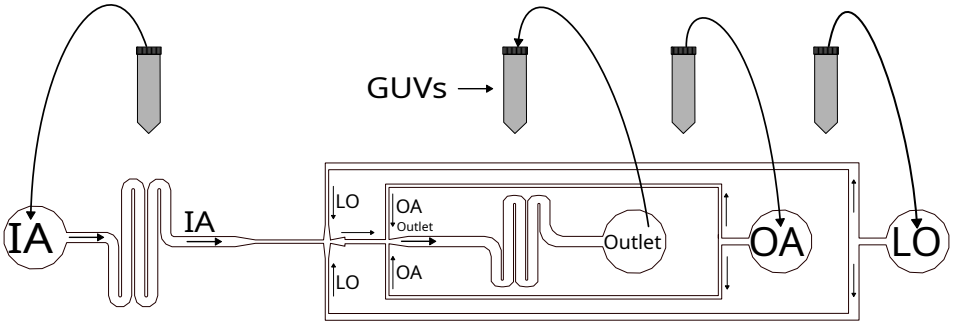

Figure 8: OLA experiment schematic. The inner aqueous phase (IA), outer aqueous phase (OA), and the lipid-oil (LO) solutions are propelled through the chip and towards the outlet. The first junction produces alternating droplets of IA and LO. GUVs are formed at the second junction. Adapted with permission from Paper I under the CC BY license.

2.5. Liposome production via hydrodynamic focusing (HDF)

The second approach based on microfluidics involved the use of a single junction chip to produce liposomes in a process known as hydrodynamic focusing (HDF). Figure 9 shows the experimental setup of the liposome production. The microfluidic chips were made out of PDMS and bonded to glass, as described in Paper I. One input was a solution of phospholipids in alcohol. The second input channel was fed with ultrapure water. A solution of phospholipids (3.9 mM dipalmitoylphosphatidylcholine (DPPC), 0.1 mM DPPG, and 1 mM of cholesterol) dissolved in ethanol (imaged with TEM) or isopropanol (for the stability assessment) was jetted into a stream of ultrapure water-based buffer (Section 3.5). As the alcohol gets diluted suddenly, the phospholipids become exposed to a predominantly water-based solvent and thus spontaneously organize into liposomes with a diameter of ~ 100 nm. These phospholipids were chosen because their T_{m} of ~ 41 °C, making it relatively easy to conduct experiments both below and above this temperature as this level is above room temperature and is easily achievable with simple tools.

In cases where calcein was loaded into the lumens of the liposomes, the resulting liquid was tangential flow filtered (TFF), if needed, using a HBM-TFF-EVs-S filter (Hansabiomed, Estonia) with a pore size of 50 nm. The purpose of the filtering was to remove the unloaded calcein from the medium surrounding the liposomes.

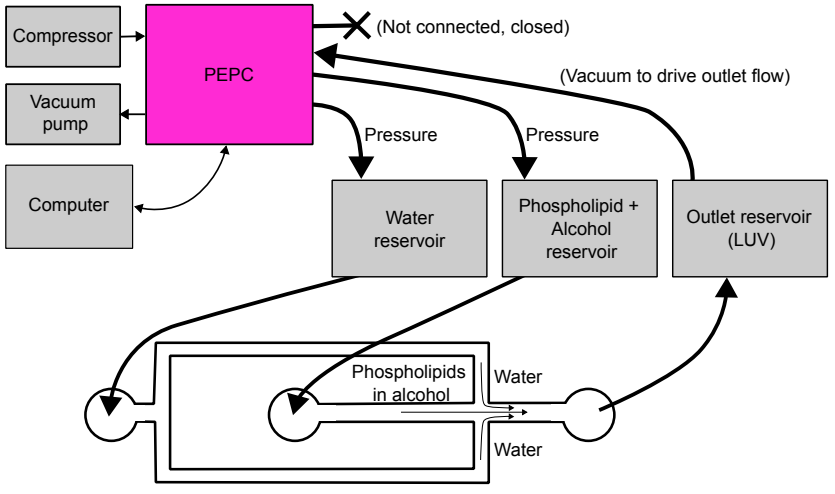

Figure 9: HDF liposome production experimental setup. A mixture of phospholipids in alcohol is jetted into a stream of ultrapure water-based buffer. Adapted with permission from Paper II under the CC BY license.

2.6. Liposome counting

One way to assess the physical stability of GUVs was to count the seemingly intact ones at different time points when the GUVs where deposited on a microscope slide and kept in a sealed chamber. To do this, GUVs containing calcein were produced and placed in a sealed 30 μL hybridization chamber. Whole slide scans were performed using an inverted microscope built around a Till iMIC body (Till Photonics/FEI, Munich, Germany) at different time points. A PlanFLN 10× (NA 0.3) objective (Olympus Corp., Tokyo, Japan) was used. An additional 2× magnification was provided by a TuCam dual camera adapter (Andor Technology, Belfast, UK) in the emission path. An iXon Ultra 897 EMCCD camera (Andor Technology, Belfast, UK) was used for image acquisition. For epifluorescence imaging, the probes were excited with a 488-nm PhoxX laser diode (Omicron-Laserage, Rodgau, Germany) and the emitted light was spectrally separated with a ZT488/561rpc polychromatic dichroic mirror (2.0 mm substrate, Chroma Technology, Bellows Falls, USA) and a BrightLine 524/628-nm dualband bandpass filter (Semrock Inc., Rochester, USA). A tiling protocol with autofocusing enabled in the Live Acquisition 2.7 software (FEI, Munich, Germany) was used to control the process. The images were stitched together using the Microscopy Image Stitching Tool (MIST) plugin for the ImageJ open-source software. A 20% overlap between the images with an uncertainty of 1% was assumed by the plugin.

After stitching of the fluorescent channel images, the GUVs were counted using an AI assisted approach. A computer vision model was trained using the Yolov5 software package from a dataset of 60 images with pixel dimensions of 640×640. The batch size was 32 images, training was carried out with 40 images and 20 images were used for validation. A deep neural network containing 379 layers with one class and a learning rate of 0.01 was trained to detect the liposomes. The Leaky ReLU activation function was used in the middle/hidden layers and the sigmoid activation function was used for the final detection layer in the neural network. Stochastic gradient descent was used as an optimization function. After training, a detection precision of about 95% was achieved. An example of the AI-assisted GUV detection is presented in Supplementary Figure S1 of Paper I.

An application, called Liposome counter (LC) (Figure 10), was developed to make the liposome counting process more ergonomic and efficient. The application combines automatic computer vision through the machine learning model described above and manual identification to count the number of liposomes and their sizes on an image. The interface contains a text field where the user is expected to enter the absolute path to the file that is being analyzed.

Figure 10: Liposome counter. A screenshot of the Liposome counter (LC) application. In this case, five eGFP containing GUVs have been manually identified on an fluorescence microscopy image.

At this stage, the user may either initiate automatic liposome detection by selecting "Calculate positions automatically" or perform manual annotation by clicking on the image to place liposome indicator boxes where none are present. Indicators are rendered as semi-transparent red rectangular overlays. Each overlay can be repositioned via click-and-drag and resized by dragging its edges. Shift-clicking an overlay records its current dimensions as the default for subsequently added overlays, whereas clicking an existing overlay removes it.

2.7. Calcein release from liposomes

To assess the stability and payload release kinetics of liposomes, a payload release experiment using calcein, a self-quenching fluorescent dye, was carried out. The fluorescence of calcein is concentration-dependent: the fluorescence increases with concentration until 4 mM, after which the molecule starts self-quenching and the overall fluorescence intensity drops as concentration increases (Figure 11). [54]

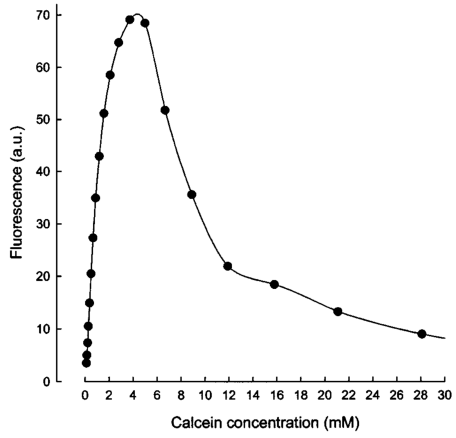

Figure 11: Calcein fluorescence vs. concentration. The fluorescence intensity of a calcein solution increases with concentration until 4 mM and then the trend reverses as the calcein starts to self quench. Reprinted with permission from Hamann et al. [54]. Copyright © 2002, Plenum Publishing Corporation.

This phenomenon makes it possible to calculate the amount of calcein released from liposomes based on Equation (2.3):

$$R = \frac{F - F_0}{F_{100} - F_0} \times 100\%, \tag{2.3}$$

where R is the percentage of released calcein, F is the fluorescence intensity at the given time point, F_0 is the initial fluorescence intensity and F_{100} is the fluorescence intensity after the destruction of all the liposomes using Triton X-100. [72]

Liposomes were loaded with a high concentration of calcein (60 mM). In this state, the fluorescence of the molecule is heavily suppressed (self-quenching). Upon the calcein release (leakage) from the liposomes, the released calcein start to fluoresce more, and thus, the overall fluorescence intensity of the solution increases. The liposome solution was diluted 1:50 so that the concentration of calcein in the space outside the liposomes could not reach higher than 4 mM even after all the calcein was released from all the liposomes. A Synergy Mx microtiter plate reader (Bio-Tek Instruments, Inc., USA) was used to measure the fluorescence intensity of the samples. Periodic measurements were automatically performed with a filter configured to excitation and emission bandwidths of 485/9.0 nm and 526/20.0 nm, respectively. To make control samples, the calcein/IA solution was also diluted 1:50, like the samples containing GUVs. To negate the effects of uncontrolled parameters, such as temperature, the fluorescence intensity values of all samples were normalized using the mean fluorescence intensities measured from the control samples at each time point. After the automatic measurement process was completed, 0.5% (final concentration) Triton-X was added to all the samples to break any remaining or still intact GUV membranes.

2.8. *EasyFlow* post-image analysis software

EasyFlow is a software developed to analyze data produced from the image analysis of droplets used as miniature reaction vessels. For example, fluorescent bacteria containing a CRISPR system with an anhydrotetracycline (aTc) toggle switch were encapsulated and incubated in droplets at different temparatures. *EasyFlow* analysis revealed that the bacterial initiation of replication was blocked by the CRISPR system at 37 °C, but not at 42 °C. The microscopy images being studied need to first be analyzed using tools such as CellProfiler™ to produce numerical data in CSV files, after which they can be used to analyze and plot the data easily using *EasyFlow*.

EasyFlow expects a comma delimited CSV or an XLSX file with a title row as an input. Each row in the input file should represent one droplet. A standard CellProfiler CSV output format is expected: sample name, volume and intensity. Droplets with the same sample name are grouped together in the analysis. The volume represents the size of the particle (cell, droplet, or liposome), but does not necessarily mean physical volume. If the input data for CellProfiler is a stack of slices, e.g. obtained from confocal microscopy, then it represents an estimated physical volume, but if the data is instead originating from a 2D image, then this value represents the area of the particle in the image. Intensity refers to the measured value obtained for a given droplet, such as the amount of green color or the number of particles detected inside it.

The user is expected to insert a threshold intensity value that is used to classify droplets as negative (below the threshold) or positive (above the threshold) results. This is useful for experiments where the intensity indicates success or failure. *EasyFlow* then plots histograms of the distribution of all the droplet intensities and droplet volumes. A scatterplot of the volume and intensity of all the particles and a scatter barplot of the intensities of each of the samples is also generated. On both scatterplots, the positive and negative particles are plotted with different colors so that the user can easily see the distribution.

Next, there is the *special-case module*, where the user can choose between a polydisperse droplet analysis and a growth heterogeneity mode. In the polydisperse droplet analysis mode, the software will plot the viability of the various samples (number of above threshold particles) compared to a control sample, if one exists. In the growth heterogeneity mode, the user can choose to plot the single cell viability and MIC probability densities or to just perform a Gompertz fit. The software is designed so that new special-case modules could be added if necessary, such as modules for antibiotic synergy analysis or time-lapse growth dynamics.

There is a *Droplets - polydisperse - Dummy.csv* file included with the source code to make it possible to quickly test the capabilities of *EasyFlow*. Figure 12 shows representative outputs produced from this dataset. Figure 12a displays

droplet intensities by sample tube as a scatter plot. Points are colored to distinguish negative and positive droplets based on an intensity threshold that the user sets manually. This plot is intended to help the user choose a threshold that will be applied throughout subsequent *EasyFlow* analyses to separate droplets where the reaction occurred from those where it did not. Figure 12b summarizes the polydisperse analysis. The horizontal axis distinguishes sample tubes. The vertical axis reports the total volume of droplets in each tube, computed using only droplets classified as positive under the manually set threshold. The thick dotted line shows the volume of droplets whereas the thin solid lines show the within-tube droplet size distribution, normalized relative to the mean size in that tube. The heights of these lines represent relative proportions of size populations and do not correspond to the absolute volume values on the vertical axis. Legend entries report the upper bound of each size bin; the lower bound equals the upper bound of the next lower, or zero for the smallest bin. Figure 12c presents a single-cell viability plot. The horizontal axis displays antibiotic concentration and the vertical axis shows the ratio of positive droplets (live cells) to negative droplets (no live cells). Antibiotic concentrations for each tube are entered manually via a text field. A regression line is fitted using Equation (1.5), allowing the experimenter to assess the goodness of fit. Figure 12d shows the MIC_{50} probability density derived from the fitted model in panel c.

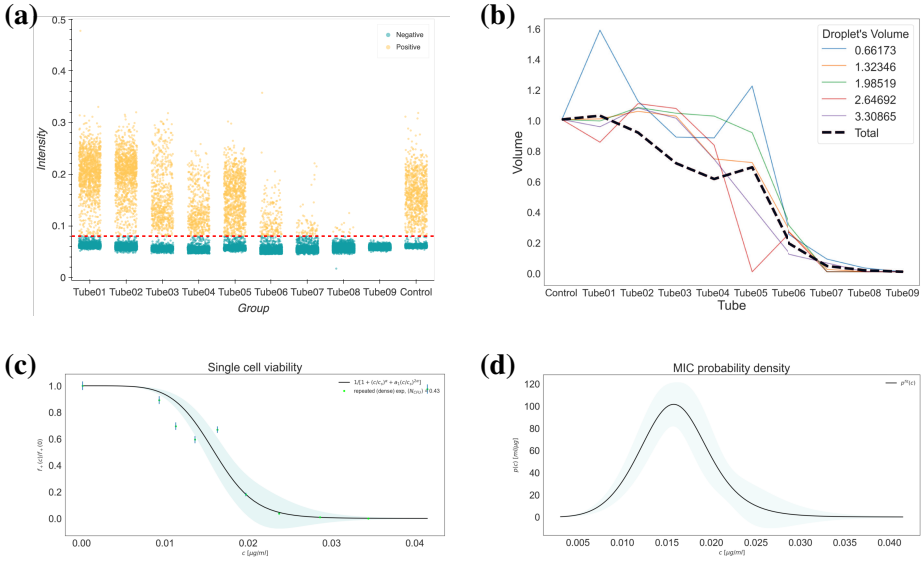

Figure 12: *EasyFlow* output data. (a) A scatterplot showing the intensity values per input label (tube). Droplets are classified as negative or positive based on a manually entered threshold value. (b) Polydisperse droplet analysis plot showing the sizes of positively classified droplets per label (tube). (c) Single cell viability plot with a fitted regression line using Equation (1.5). (d) Probability density plot of MIC values across bacterial strains. In this figure, MIC denotes MIC_{50} (the concentration inhibiting 50% of isolates).

3. RESULTS AND DISCUSSION

Reliable pressure control is essential for reproducible microfluidic liposome production, and high-throughput experiments also require ergonomic tools for quantitative analysis. This chapter therefore starts by presenting enabling pressure-control developments: first, a software interface for multi-channel pressure and vacuum operation (pressure controller software (PCS)), then a low-cost multi-channel pressure regulator (piezoelectric pressure controller (PEPC)), followed by a performance characterization of the regulator.

The experimental results are then presented in two parts. First, the production of GUVs via OLA using an off-the-shelf vacuum source, enabling microscopy-based characterization, on-chip payload loading and subsequent stability and passive leakage measurements. Second, because the OLA-produced GUVs exhibit substantial passive release, the chapter shifts to HDF to produce smaller, oil-free liposomes and to assess their size distributions and stability, using the PEPC for stable multi-channel pressure control. Finally, the chapter concludes with a complementary post-image analysis tool that streamlines the evaluation of droplet- and vesicle-based experiments.

3.1. Pressure controller software (PCS)

To have an ergonomic pressure control interface for sources / regulators in microfluidic experiments, a *Node.js* based software package named the PCS was developed. The software has two modes: one to handle multiple instances of Fluika pressure/vacuum generators connected via universal serial bus (USB) simultaneously, and another mode to control the PEPC. The graphical user interface (GUI) in both modes is similar and allows the experimenter to conveniently change and monitor multiple pressure channels simultaneously.

3.1.1. Fluika mode

The pressure generator used for the OLA experiments (Section 3.4) lacked an ergonomic control interface. To address this, a custom controller application was developed as part of this thesis.

The Fluika device is connected to a PC and communication with it is handled via a serial protocol. A *Node.js* based software with a browser-accessible GUI was implemented using a client-server architecture. The *Node.js* application communicates with the pressure source using the *serialport* library. The GUI is exposed at the URL `localhost:7005`.

The GUI provides a pressure controller unit view with a drop-down menu for selecting the appropriate serial port. After connection, the pressure controller view displays an input field for the user to specify the desired pressure value, while the current pressure reported by the pump is displayed in real time. There is a text

field for the user to assign a custom name for the device. The software supports the simultaneous control of multiple Fluika devices, each connected to a different USB port.

This enables an experimenter to monitor and quickly change the pressure target values for multiple channels at the same time while reducing mistakes, as custom name labels make it easier to keep track of which input field in the GUI controls which pump. The application also contains a safety feature that shuts down the power to the Fluika device in case it detects an error. This is necessary to prevent the device from flooding the microfluidic chip with the wrong liquid, especially the LO solution during OLA, which can ruin the chip.

3.1.2. PEPC mode

The PEPC control mode GUI features all the same ergonomic features as the Fluika mode with minor differences due to the fact that the PEPC is a single device featuring multiple pressure output channels and needs calibration. In this case, there is a single dropdown menu at the top of the screen that the user needs to select a serial port to connect. Once connected, four controller views are displayed, one for each channel on the PEPC (Figure 13).

Figure 13: Pressure controller application. There is a dropdown menu at the top that is used to select a serial port to connect to. Four channel controller views are shown when a device is connected. Reprinted with permission from Paper II under the CC BY license.

It is possible to perform calibration actions on all the channels together and separately. The first time the application is connected to a PEPC, it will automatically prompt to perform initial calibration for all channels. PEPC calibration is a three

step process. First, to correct for the static error of the analog to digital converter (ADC) at 0 mbar, the "ADC offset" calibration is performed by disconnecting and opening all input and output channels and then recording the voltages reported by the valves. 25 measurements are averaged for each channel to obtain the calibration offset values.

Second, "calibrating all channels by scanning" is done by connecting both input channels (pressure and vacuum) with all the output channels closed and then setting varying target pressure values and recording the resultant reported voltages. The correspondence between the requested and reported resultant pressures are plotted for each channel and can be viewed by clicking on the "Chart" button in the respective channel controller view. These calibration curves are used to perform a reverse lookup (via interpolation) to adjust the voltage that is sent to the valve when the user requests a given pressure value. As an example, if during calibration it was determined that sending a request to the PEPC for 20 mbar resulted in an output pressure of 15 mbar, then it follows that in order to obtain an output pressure of 15 mbar, the application must request 20 mbar from the PEPC instead. The software records the calibration values in the local storage of the browser and uses them to make sure that the user gets the desired output pressures. The limits of the achievable output values are also determined and the GUI adjusts the minimum and maximum available pressure values for each channel so that the user cannot request impossible values.

Third, each channel controller contains an additional "Set as zero" button that allows the user to set an additional offset to the scale. The purpose is to allow the user to correct for any pressure differentials caused, for example, by the liquid column pressure in the tubes leading from reservoirs into microfluidic chips.

Overall, the PCS contains everything that an experimenter might need to conduct experiments with both the PEPC pressure regulator, as well as the Fluika miniature pressure regulation kit. In addition, it also allows for infinite customization by virtue of by being open-source.

3.2. PEPC pressure regulator

This section describes the hardware and the embedded software of the PEPC as well as characterizes its performance in the context of its intended application and compares it to some of its closest analogs.

3.2.1. Pressure regulator design and construction

Since the stability of the pressure source can be crucial for the quality of the results of a microfluidic experiment and one of the stated aims of this thesis is to increase the accessibility of microfluidic liposome production, the design of an open-source, high-stability pressure regulator that could compete with the relatively expensive commercial analogs available on the market was undertaken. The custom pressure regulator, named the PEPC, was designed and constructed from

commercially available "off the shelf" components (Figure 14). The design of this pressure regulator is described in detail in Paper II. Briefly, it is a device consisting of four voltage controlled proportional pressure regulation valves (*Tekno plus vakuum*, Hoerbiger AG, Switzerland), an Arduino-based microcontroller and a custom mainboard with an analog to digital (ADC) and a digital to analog converter (DAC) device. Internally, the system uses analog signals between 0 V and 10 V to communicate the target pressure to the pressure regulation valves and the current output pressure measured by the valves is communicated to the controller via the same method. Externally, the PEPC communicates with a computer via a serial connection (USB) to a laptop computer. It can control pressure in the range from -1000 mbar to 1000 mbar with an accuracy of 0.7% of the requested value, given powerful enough pressure sources.

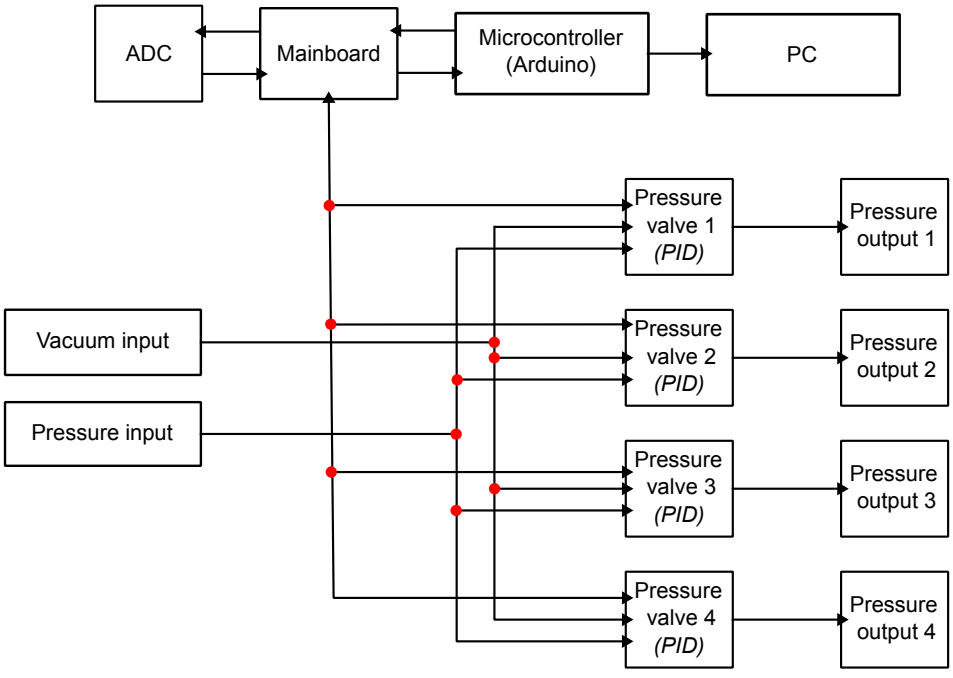

Figure 14: Main components of the pressure regulator. Main components and connections inside the device. Reprinted with permission from Paper II under the CC BY license.

The pressure regulator valves internally use a PID control algorithm that is pretuned by the manufacturer. This algorithm is used only inside the valves and is actually hidden from the control electronics in the PEPC, however, it affects the response characteristics of the controller.

The PEPC was deliberately over dimensioned in terms of its maximum output pressures for the specific microfluidic experiments performed as part of this thesis because the initiation of the experiment requires more extreme conditions that

steady state operation. First, to displace trapped air, liquid must be driven through the channels with sufficient force to overcome the adhesion of bubbles to channel walls. In the case of symmetrical chip designs, such as those used in this work, liquid must flow through both sides of the chip simultaneously. If one side fills faster, air can get trapped on the other side because a liquid plug forms at the junction where the two channels meet, making purging even harder. Excessive flow rates, however, can lead to cavitation and generate new bubbles inside the chip, which is also counterproductive. The solution to this problem is to quickly increase and decrease the flow rates to dislodge the trapped air bubbles. All this means that the system must be capable of high flow rates during priming, even though only low flow rates may be required during the actual experiment.

However, for experiments, precise control of low flow rates can be essential. In GUV production, three relative flow rates need to be balanced exactly and even small perturbations can disrupt proper operation. In the case of HDF, the required precision is less strict, but fluctuations of the relative flow rates will lead to decreased homogeneity of the final product. [156, 164]

3.2.2. PEPC firmware

Since the PEPC contains an Arduino, the firmware was written for it using the official Arduino IDE. It was designed to read input commands using Serial.read(), if there are any to be read, and immediately apply the appropriate voltages to the valves. Then it would report its current state back to the PC by sending a JSON formatted string using Serial.write().

The format of the JSON packet is like this: {“A”: 13520, “B”: 13432, “C”: 14112, “D”: 13580, “A_r”: 15000, “B_r”: 0, “C_r”: 0, “D_r”: 0, “multiplier”: 0.000187505722045}. This describes the whole current state of the PEPC. “A” indicates the current measured pressure value (voltage) in output channel A. A_r is the current requested pressure value for output channel A. The multiplier value is the value that the current measured pressure value should be multiplied by to find the corresponding voltage between 0 V and 10 V where 0 V, 5 V and 10 V indicate -1000 mbar, 0 mbar and 1000 mbar of relative pressure, respectively.

The firmware is designed so that it holds no other configuration than the current requested integer values (between 0 and 65535) for each channel. All conversion to voltages and calibration is handled on the side of the controlling PC. The JSON packet also includes a conversion multiplier to quickly convert reported output values to approximate voltage values. This multiplier never changes and further corrections must be performed on the side of the coordinating computer by calibration, as described in Section 3.1.2, if high accuracy is required.

3.3. PEPC performance characterization

The central design goal of the PEPC was to provide a highly stable input pressure source for microfluidic experiments where small fluctuations can cause significant

disturbances in the quality and quantity of the product of the experiment. Therefore, it was important to measure its stability and responsiveness. An experiment was devised in which a script repeatedly set predetermined pressure targets and recorded the output until stabilization. A signal is considered stabilized when the average standard deviation of the signal measured over 5 s has dropped below 0.75 mbar. The standard deviations of stabilized output pressures after transitioning to various target pressures are shown on Figure 15. It is apparent that the standard deviation (SD) of the pressure does not tend to be higher than about ± 0.15 mbar and the average SD is ± 0.12 mbar, corresponding to a stability of 0.006% full scale (FS). This is similar to the closest commercial analogs of the Elveflow OB1^{TM} MK4 (–900 to 1000 mbar version), the Fluigent MFCS^{TM} and the Biophysical tools I^{2}CS^{TM} with their respective reported stabilities of 0.005% FS, $< 0.1\%$, and 0.007% FS.

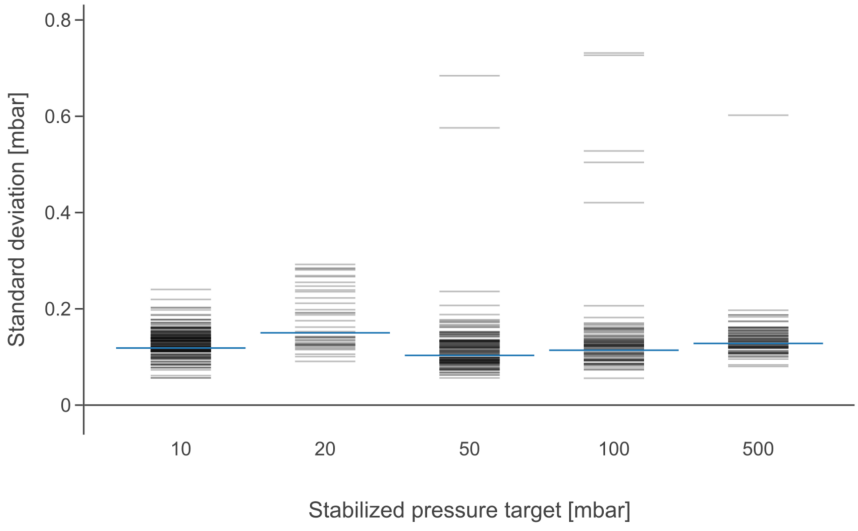

Figure 15: PEPC stability. SDs of 5 second-long samples of stabilized pressure values measured at various target pressures. The blue lines represent average SDs. Translucent black lines represent SDs from individual measurements. Reprinted with permission from Paper II under the CC BY license.

While the self-reported stability of the PEPC is impressive, it is also important to gauge the realiability of those self-reported values. Table 2 lists the average differences between the values reported by the PEPC and a calibrated differential manometer (Kane 3500-5, Kane International Limited, Welwyn Garden City, UK). Each difference listed is an average of five reading differences measured simultaneously by the PEPC and the manometer. To calculate the reporting error values, the value reported by the PEPC was subtracted from that obtained using the manometer. The $\pm$ values indicate SD values calculated from 5 samples. The reporting values are normalized so that the reporting error at 0 mbar is defined as

0. This is justified as the user can perform the same normalization using the "Set as zero" button for the corresponding channel in the GUI of the PCS. The reporting errors appear to increase together with the distance of the reported pressure value, but never reaches above 0.7% of the reported value within the ±380 mbar relative pressure measurement range of the manometer, which is adequate to represent the accuracy of the device for many low pressure applications. [156, 48, 148, 99, 163, 144]

Table 2: Reporting error of the PEPC compared to a calibrated manometer. Reprinted with permission from Paper II under the CC BY license.

Requested value (mbar)	**Average reporting error** (mbar)	**Average relative reporting error (%)**
−380	2.55 ± 0.10	0.67 ± 0.03
−200	0.62 ± 0.16	0.31 ± 0.08
−50	0.10 ± 0.13	0.20 ± 0.26
0	0.00 ± 0.08	N/A
50	-0.09 ± 0.13	-0.19 ± 0.25
200	0.47 ± 0.17	0.23 ± 0.08
380	1.48 ± 0.11	0.39 ± 0.03

The last characteristic of the PEPC that was studied is the response speed when the target pressure changes. Figure 16 shows how much time the pressure regulator takes to transition between various target pressure values. Transitioning, in this case, is defined as the point in time from which the average values recorded during the first, third, and fifth seconds following that time point are within ±0.25 mbar (SD) of each other. The transition time of the PEPC is typically between 3 and 10 s. This is relatively slow compared to the commercial analogs, but is good enough for most microfluidic particle production experiments that do not require significant fast changes to the input rates once the system has reached the operational regime.

The varying transition and stabilization times are caused by the unpredictability of the PID algorithm in the valves. The transition time is dependent on the particular values that are transitioned between and also to some unknown extent on the history of the pressure chart before the start of the transition process (the integral term). It is unknown because the PID parameters used in the valves are hidden by the manufacturer.

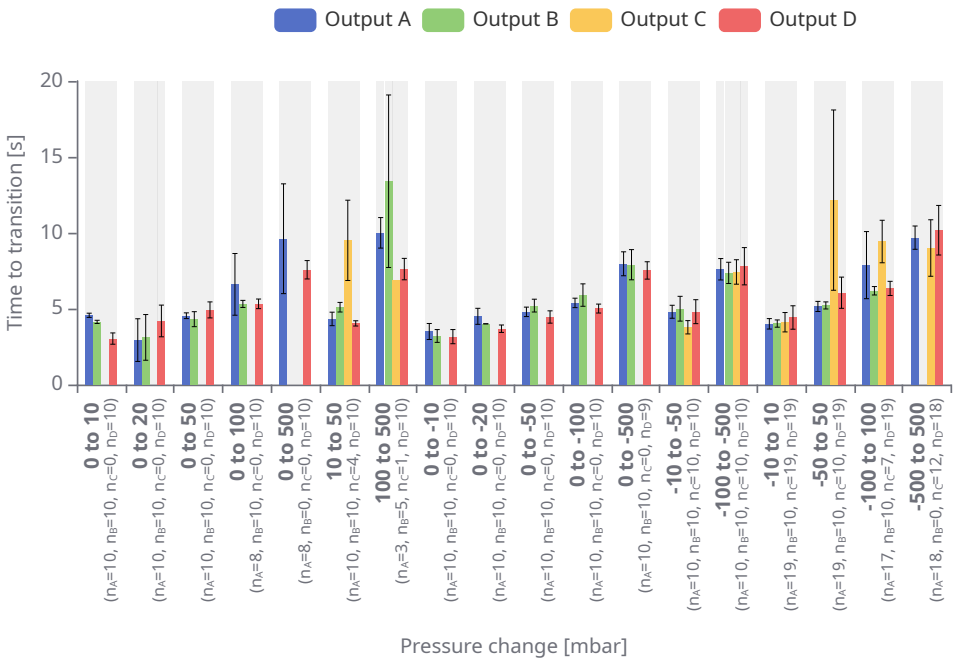

Figure 16: PEPC pressure response speed. Time taken to transition between various target pressure values. Outputs A, B, C and D correspond to the four valves in the PEPC. Reprinted with permission from Paper II under the CC BY license.

In addition, the accuracy of the pressure reported by the PEPC was measured by comparing the pressure readouts against the manometer.

Table 3 shows a comparison of the PEPC *versus* some commerial alternatives, including the Fluika VG350 used in the OLA experiments below (Section 3.4), is an example of. The values listed in Table 3 are specifically calculated for this table so that it would be possible to compare it to commercial and open-source analogs. The data for the Elveflow OB1^{TM} was retrieved from *OB1 MK4 Flow controller* [103]. The Fluigent MFCS^{TM} values are from *Microfluidic Flow Control System - Fluigent* [88].

The PEPC exhibits similar stability and accuracy to those of the alternatives. The settling time is longer compared to commercial alternatives other than the Fluika system, which is comparable in that regard. Moreover, the stability of the PEPC is also significantly superior to that of the Fluika device. Moreover, the total parts cost was about 4,000 €, roughly one third of comparable commercial systems and even less than the cost of four Fluika units.

Table 3: Pressure regulators. Adapted with permission from Paper II under the CC BY license.

	PEPC	**Elveflow OB1™**	**Fluigent MFCS™**	**Fluika miniature pneumatic control kit**	**Biophysical tools P²CS™**	[120]	[39]	[44]
Pressure range [mbar]	−1000 to 1000	−900 to 1000	0 to 1000	−350 to 500	−1000 to 1000	0 to 690	0 to 2200	0 to 2000
Stability	0.006% FS	0.005% FS	<0.1%	1 to 1.5% FS	0.007% FS	0.01% FS	0.3% FS	0.02% FS
Response time [ms]	69	10	10	-	4	-	-	-
Settling time [ms]	2100	50	-	10000	5 or 17	-	-	-
Min increment (step size)	0.05% FS* 0.0015% FS (theoretical)	0.0064% FS	0.03% FS	0.5% FS	0.006% FS	-	-	-
Accuracy	<0.7% **	2.5%	0.25% FS	0.2% FS	0.5% FS	0.16% FS	0.37% FS	0.09% FS

* Arbitrarily limited in software.
** In the range of −380 — 380 mbar.

3.4. GUV production via OLA

Despite repeated attempts, the success rate of the microfluidic chip outlet channel coating with PSS and PDADMAC never exceeded $\sim 10\%$. For this reason, precoated chips were obtained from Dr. Naresh Yandrapalli (author of Yandrapalli et al. [156]) and they were used for all GUV production experiments reported here.

At first, GUVs (POPC, which is a neutral charge phospholipid) were produced using the OLA approach, enabling precise control over the distribution of particles or other materials relative to the membrane (Paper I). Figure 17 shows two images of the production of GUVs using OLA, where it is possible to see how 5 mM calcein (yellow) filled liposomes are formed in the experiment. Some of the liposomes contain a large amount of octanol (as evidenced by the white crescent shapes) while some are relatively oil-phase-free. It was not possible to reduce the amount of octanol flow significantly due to the low stability of the vacuum generator and the way that the relative pressures of the input channels were controlled by hand in the given experimental setup (Figure 8). The relative pressures would constantly change as the amount of liquid in the reservoirs dwindled, changing the relative pressures and flow rates. If the LO flow rate fell too low, liposome production would stop and it would be necessary to increase it significantly above the normal operational rate in order to restart the production. The experiments involving this liposome production method were driven by Fluika pressure pump units and not the PEPC, as the latter device was developed as a direct consequence of the challenges encountered during the OLA experiments.

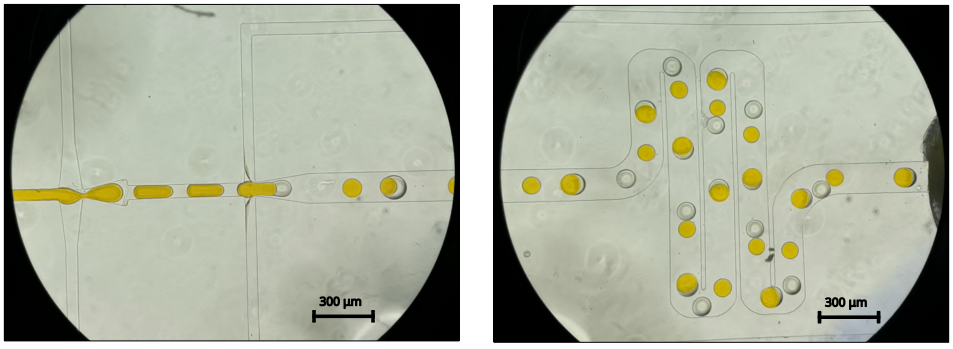

Figure 17: OLA production. A vacuum pump pulled the liquids through the chip and towards the outlet (right side). The formation of alternating water and oil droplets in the first (left) junction is seen on the optical microscopy images (IA is yellow due to a calcein dye) and GUVs were formed at the second junction. Adapted with permission from Paper I under the CC BY license.

Figure 18a illustrates the appearance of ultrapure water containing liposomes under stationary conditions. The crescent shapes that were visible in the outlet channel during production (Figure 17) had disappeared because the calcein has a lower

density than water and therefore it has risen to the top of the liposome. Since optical microscopy imaging is performed from the above or from below, depending on the microscope used, the oil is therefore not as easily visible in such static cases. The crescent was visible in the outlet channel of the chip because the flow of liquid caused the calcein to move towards the leading edge of the liposome. The histogram of the size distribution, determined with the aid of LC, with the the average diameter of $92 \pm 6\ \mu$m (SD, PDI $= 0.004$) of these GUVs is shown in Figure 18b. The size distribution of the GUVs is rather narrow. This is desirable since the opposite case of a highly heterogeneous liposome population would create unnecessary noise in liposome stability and payload release experiments.

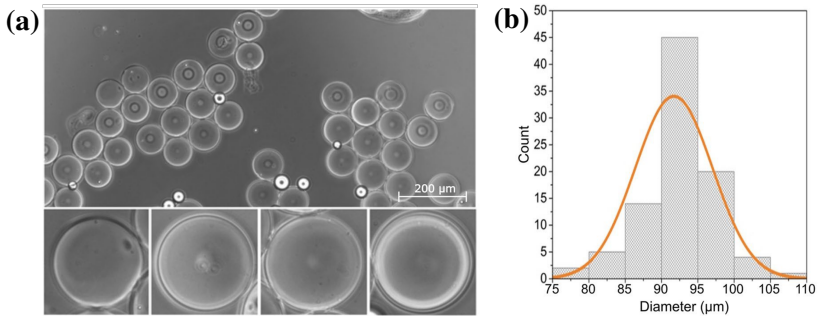

Figure 18: GUVs. (a) Optical microscopy image of GUVs in a droplet placed on a microscopy slide . Size of zoomed-in insets is $100\ \mu\text{m} \times 100\ \mu$m. (b) Diameter histogram of GUVs ($n = 91$), the average diameter is $92 \pm 6\ \mu$m (SD) corresponding to a PDI of 0.004. Graph bars show the relative amount of GUVs with diameters in the respective $5\ \mu$m range. The orange line represents the Gaussian fit of the data. Reprinted with permission from Paper I under the CC BY license.

3.4.1. GUV physical stability

To gauge the practical value of the GUVs and to provide a baseline for payload release experiments, their physical stability was studied by assessing their degradation and leakage rates. For this, eGFP containing GUVs were produced and their stability was studied in two ways, first by counting the number of liposomes and then by a calcein release assay. Figure 19a shows the results of a liposome counting experiment (initial count ~ 1000) in a sealed chamber on a microscope slide. After 140 h, the number of liposomes fell by $\sim 80\%$ following an exponential decay curve with a half-life of $\sim 61 \pm 2$ h (standard deviation of mean). Figure 19b depicts a fluorometric calcein release experiment where the liposomes were kept in a sealed microtiter plate and the fluorescence intensity of the solution was measured periodically to calculate the amount of payload released from the liposomes. The payload release percentage again followed an exponential path. 50% of the payload had been released after only 2 h and after 24 h, 90% of the calcein had been released (the rest of the release occurred after treatment with

Triton X-100). From these results it is apparent that the release rate of calcein exceeds the rate at which the liposomes disappear. It was concluded that the GUV membranes are significantly permeable to calcein (even without external stimuli) and that the high baseline payload release rate from these POPC liposomes makes it difficult to conduct externally triggered payload release experiments as there is little time to go through all the steps, which may take tens of minutes and even hours in some cases. Since the temperature of POPC is -2 °C and the experiments were performed at ambient (room) temperature, the GUV membranes were in the liquid crystalline phase during these stability experiments. Since this phase is inherently leaky compared to the gel phase, it is possible that GUVs with a higher T_{m} could be more stable. This was not tested, but could be considered as an option for future research. [19, 143, 86]

An interesting observation relating to the stability of the GUVs is that they would start to rapidly break down when the liposome containing solution was dissolved 1:7 (volume:volume) or more with a liquid that had not been mixed with 1-octanol beforehand. Combined with the fact that the liposome containing solution flowing out of the chip will inevitably contain some dissolved octanol due to the nature of the OLA method, this suggests that the octanol, although being almost insoluble in water (solubility of 0.3 g/L), will start to rapidly diffuse out of the liposome membranes when the concentration in the surrounding aqueous solute is low enough, disrupting their integrity. [46]

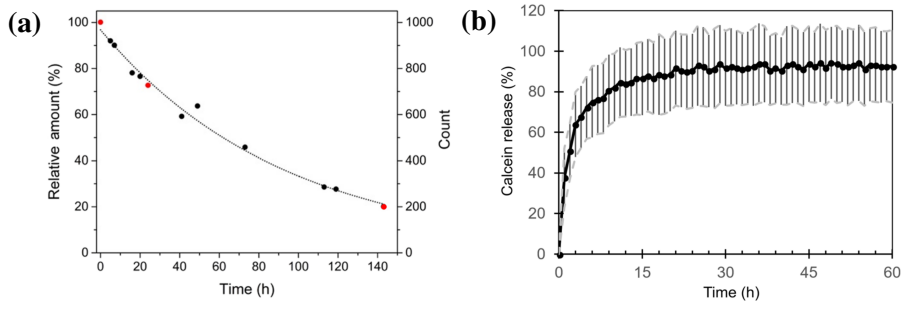

Figure 19: GUV stability. (a) Disappearance of GUVs in a chamber over time (100% GUVs at $t = 0$). The chart follows an exponential decay curve with a half-life of $\sim 61 \pm 2$ h (standard deviation of mean). Images taken at the three time points indicated in red are shown in Supplementary Figure S2 of Paper I. (b) Calcein release measured via fluorescence assay. After the first 24 h of the experiment, 90% of the calcein was released. Reprinted with permission from Paper I under the CC BY license.

3.4.2. Encapsulation of payloads into GUVs during production

In parallel with the GUV stability studies, the payload encapsulation capabilities of the OLA method were also tested. This approach naturally allows for easy

insertion of various substances, including nano- and microparticles, into the giant liposomes with a high loading efficiency during their formation unlike most other methods, where the liposomes are formed first and the payloads are inserted separately or where the encapsulation happens by random chance (see Table 1).

In this case, microscale fluorescent magnetic particles or eGFP were added to the IA solution (as in Figure 8) and the experiment was otherwise performed as described in Section 3.4. Figure 20a shows enhanced green fluorescent protein (eGFP) and Figure 20b fluorescent magnetic microspheres of 3.2 μm diameter loaded inside the lumens of the GUVs, demonstrating the successful loading of both nano- and microscale objects into the GUVs. The corresponding size distributions of the loaded GUVs are shown in Figures 20c and 20d, respectively. Analysis with the LC utility shows standard deviations of 13 μm and 6 μm (Figures 20c and 20d), similar to the 6 μm standard deviation of the non-loaded GUVs in Figure 18b. From these distributions, the PDIs are 0.009, 0.004 and 0.004, respectively. This provides further indication that the OLA method is suitable when GUVs with homogeneous size distributions are desired.

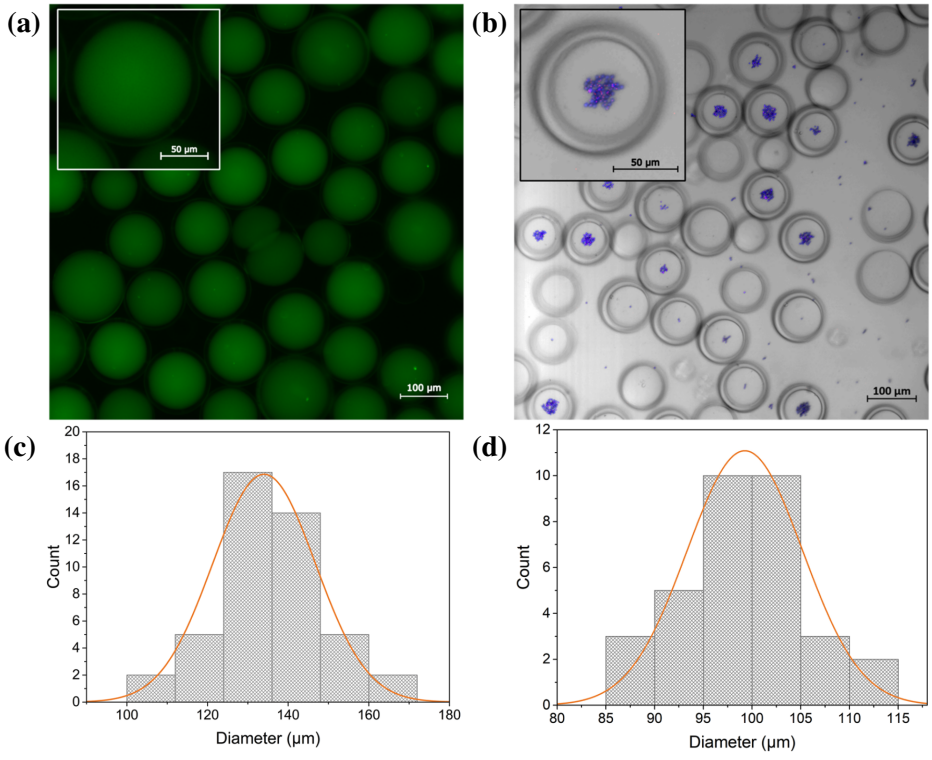

Figure 20: GUVs loaded with nano- and microscale payloads. (a) GUVs containing eGFP under fluorescence microscopy. (b) GUVs loaded with fluorescent magnetic microparticles imaged with confocal microscopy. (c) Histogram of the size distribution of the eGFP containing liposomes ($n = 45$, average diameter of 134 ± 13 μm (SD, PDI $= 0.009$)). (d) Histogram of the size distribution of the magnetic particle containing GUVs ($n = 33$, average diameter of 99 ± 6 μm (SD, PDI $= 0.004$)). Both histograms were obtained by measuring the diameters of the GUVs directly from the microscopy images. Orange curves are the Gaussian fittings of the histograms. Adapted with permission from Paper I under the CC BY license.

3.5. HDF liposome production and SUV/LUV stability

Because the GUVs were determined to be suboptimal in terms of stability for the purposes of studying payload release, smaller and potentially more stable liposomes were produced using a HDF method. This approach is much simpler than the OLA method as there are only two input liquids, making it easier to control the experiment, and there is no need to functionalize the channels of the microfluidic chip. The liposomes are oil-phase free and more stable due to their three orders of magnitude smaller size of around 100 nm, which unfortunately makes them not observable under an optical microscope and therefore makes it more difficult to conduct localized payload release experiments. If the liposomes were visible with an optical microscope, it would be much easier to analyze the results of such experiments as it would be possible to directly observe any morphological or fluorescence changes in the liposomes.

Figure 21a shows the HDF chip during the production process. The jet of phospholipids dissolved in ethanol was focused by adjusting the relative pressure values of the two input and one output channel at the beginning of the experiment and remained constant until the phospholipid solution ran out after about 10 min. For these experiments, the PEPC was used, unlike the OLA experiments, where a Fluika pressure pump was used instead. The higher stability of the pressures driven by the PEPC compared to the Fluika pump surely served to make the size distribution of the resulting liposomes narrower as the flow rate ratio of the two input liquids influences the size of the liposomes produced in the HDF experiment. Figure 21b shows the results of a DLS measurement of a sample of SUVs/LUVs produced using the HDF method, with ethanol as the solvent for the phospholipids, and filtered using TFF. There are three size populations of particles: one at ≈ 80 nm one at ≈ 180 nm and another at ≈ 420 nm. The widths of the peaks are satisfactory, with clearly distinguishable populations. The PDI of this sample is relatively high at 0.2489 due to the multimodality of the size distribution; however, it is satisfactory for the goals of this research (creating the preconditions for the study of payload release kinetics from magnetic liposomes), as it is a straightforward process to filter the liposomes to isolate the desired peak of the size distribution if needed. If the other peaks were to be filtered out, the PDI would fall to about 0.02, 0.03, 0.01 for the individual peaks. TEM imaging results, shown in Figure 21c confirm the size distribution determined using DLS. SUVs created using the HDF method were also studied for their physical stability. The results showed that the smaller (hundreds of nm diameter) and octanol-free DPPC (neutral), DPPG (negatively charged) and cholesterol containing liposomes were much more stable compared to the ~ 100 μm diameter POPC GUVs obtained from the OLA experiments. Over the course of four days at 4 °C, the concentration dropped from 220×10^6 particles/mL to 210×10^6 particles/mL in an experiment where the bimodal liposome size distributions were at ≈ 200 nm

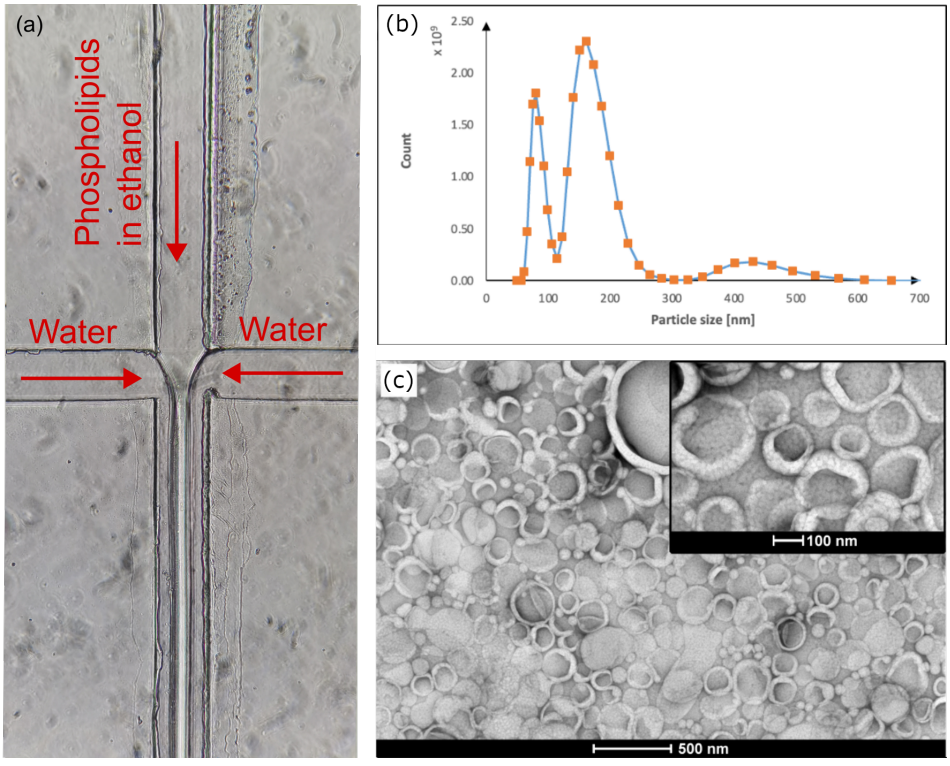

Figure 21: HDF liposome production results. (a) Bright field image of the microfluidic chip during operation. (channel width is 170 μm) (b) Size distribution of the liposomes measured using DLS. (c) Negative-stained TEM image of the produced SUVs. Adapted with permission from Paper II under the CC BY license.

and ≈ 430 nm (isopropanol was used as the phospholipid solvent in this case) according to DLS measurements. This change of $\approx 5\%$ of the concentration over four days indicates more than good enough stability to perform various experiments with them: this level of stability is sufficient for assays that can take several hours or even days for the active steps in addition to preparation times, such as payload release assays or membrane protein synthesis experiments. [91, 101, 143, 140]. In the case of the GUVs, the same kind of drop in the number of liposomes occurred already after 2 to 3 h and the amount of calcein released after 2 h was already 50% of the original amount. Part of this change in stability may be due to the significantly higher T_m of $\sim 41\,^\circ$C compared to the $-2\,^\circ$C of the GUVs.

3.6. Post-image analysis of droplet experiments with *EasyFlow*

In the same spirit as the PEPC, which was introduced as a solution to improve the accessibility and stability of microfluidic operation, the LC served as a practical tool for liposome counting within the scope of this work. However, LC is not suited to high-throughput or to cross-experiment comparability. To meet those

needs, standardized post-image pipelines (pipeline as a software workflow protocol) were established, and their outputs are processed in *EasyFlow* to provide threshold-based classification, polydisperse summaries, and growth-type metrics. The pipelines are:

1. Droplet detection and mean fluorescence measurement using CellProfiler™,
2. Droplet and fluorescent object detection in fluorescent images using CellProfiler™,
3. Droplet and object detection in brightfield images using a combination of Ilastik and CellProfiler™.

The first pipeline is designed to track the change of the intensity of a fluorescent signal in droplets, while the second pipeline can be used to observe the number of fluorescent particles per droplet over time. Both of these rely on fluorescence to analyze micro-compartments. These pipelines have potential to be applicable for the analysis of payload release experiments from liposomes, but only in the case of GUVs, since SUVs and even LUVs are too small to be imaged with sufficient resolution (for the corresponding experiments), and therefore they are not discussed further in this thesis.

The most pertinent one of these pipelines for the goals of this thesis is the third one, based on its potential use for the analysis of magnetic liposome images. It enables the analysis of the encapsulation of small particles inside droplets, as well as liposomes. An example of the results of an experiment utilizing this pipeline is shown in Figure 22a. In this case, microplastic beads were encapsulated in droplets and imaged using an optical microscope. The images were processed using the machine learning image processing software named Ilastik to produce a microbead location probability map image. CellProfiler then used this probability map to produce the intensity value for each droplet. CellProfiler works by finding the droplets and then determining the color intensity in the detected droplets. The result was a histogram showing the distribution of how many microplastic beads were encapsulated in droplets. The histogram revealed that most commonly the droplets contained 3–4 beads and that the encapsulation yield generally followed the Poisson distribution as shown in Figure 22b. A similar analysis might in the future be performed on magnetoliposomes in order to better understand the effect of the number of embedded magnetic particles on payload release dynamics.

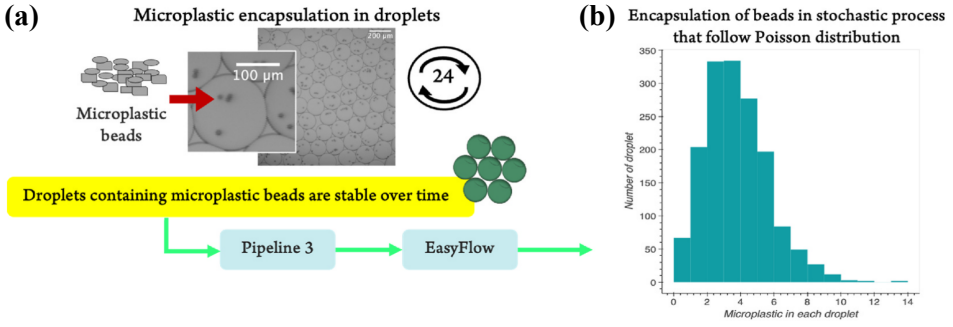

Figure 22: ***EasyFlow*** **pipeline 3 results.** Microplastic beads encapsulated in droplets analyzed using using a combination of Ilastik and CellProfiler^{TM}. Reprinted with permission from Paper III. Copyright © 2025 Elsevier B.V.

4. CONCLUSIONS AND OUTLOOK

This thesis set out to enable localized payload release from liposomal carriers by first building reliable ways to make, control, and measure the vesicles themselves. The central result is a set of methods that make microfluidic liposome fabrication and quantitative readouts reproducible enough to support future studies of remote triggering.

While the original aim of developing magnetically responsive liposomes for controlled release remains to be fully realized, this work established critical methodological foundations. Paper I established on-chip production and optical characterization of GUVs and quantified their stability and passive leakage. Paper II delivered a stable, multi-channel pressure regulator and control software that improved the reliability of flow-driven fabrication. Paper III provided a practical route from microscope images to statistically interpretable quantities for droplet and vesicle experiments.

GUVs production was demonstrated and a passive-leakage baseline was established for GUVs ($\sim 90\%$ calcein was released within 24 h, with a liposome half-life of $\sim 61 \pm 2$ h). Nanoscale liposomes with bimodal size distributions near ≈ 200 nm and ≈ 430 nm that remained stable over days (only ≈ 5 % concentration decrease over four days) were produced using HDF, while the development of a four-channel pressure controller enabled stable operation using negative and positive pressures simultaneously to drive experiments with multiple input liquids. The post image analysis software *EasyFlow* provided a standardized image to numbers route for droplet and vesicle experiments by converting microscope images and CellProfiler outputs into decision-ready plots and metrics. These capabilities are applicable to vesicle payload readouts and to future triggered-release assays that rely on intensity-based classification. Together with the pressure-stable fabrication workflows, this closes the loop from on-chip production to quantitative readouts and defines consistent acceptance criteria for leakage baselines and for subsequent field-triggered release tests.

The integration of magnetic responsiveness (with magnetic particles) into liposomal systems remains an unresolved methodological challenge for the development of the necessary model systems. Although the existing literature often presents (magneto)liposome fabrication as straightforward, their reliable and reproducible preparation is technically demanding in practice. One way to approach the issue might be to produce GUVs via OLA, introducing the magnetic nanoparticles via the LO liquid. The PEPC being significantly more stable compared to the system used in Paper I would make it possible to repeatably produce homogeneous GUVs of varying sizes (to study how the liposome size affects the payload release). Unfortunately, the issues of octanol contamination of the liposome membranes and the stability of the GUVs would remain. However, even with the instability, it might be possible to study the payload release dynamics and their size dependence of the liposomes under very low frequency external

magnetic fields with well developed experimental pipelines. Alternatively, magnetic liposomes could be produced using yet another method, such as TFH. These liposomes might then be used to test the payload release dynamics under low frequency magnetic fields. These liposomes would likely not be as homogeneous as those that can be produced using microfluidics (OLA and HDF), but the size dependence of the payload release dynamics could still be studied by extruding the liposomes to different sizes and then accounting for the difference.

Building on the methodologies developed here, future research can focus on incorporating magnetic nanoparticles into liposomes and validating controlled release under external stimuli. The tools and techniques presented in this thesis provide a valuable platform for these advancements.

BIBLIOGRAPHY

[1] M. Abramowitz, K. R. Spring, H. E. Keller, and M. W. Davidson. “Basic Principles of Microscope Objectives”. *BioTechniques* 33.4 (2002), pp. 772–781. https://doi.org/10.2144/02334bi01.

[2] S. Adepu and S. Ramakrishna. “Controlled Drug Delivery Systems: Current Status and Future Directions”. *Molecules* 26.19 (2021), #5905. https://doi.org/10.3390/molecules26195905.

[3] M. Aghaaminiha, S. A. Ghanadian, E. Ahmadi, and A. M. Farnoud. “A machine learning approach to estimation of phase diagrams for three-component lipid mixtures”. *Biochimica et Biophysica Acta (BBA) - Biomembranes* 1862.9 (2020), #183350. https://doi.org/10.1016/j.bbamem.2020.183350.

[4] T. Akyazi, L. Basabe-Desmonts, and F. Benito-Lopez. “Review on microfluidic paper-based analytical devices towards commercialisation”. *Analytica Chimica Acta* 1001 (2018), pp. 1–17. https://doi.org/10.1016/j.aca.2017.11.010.

[5] M. Aleksanyan, H. A. Faizi, M.-A. Kirmpaki, P. M. Vlahovska, K. A. Riske, and R. Dimova. “Assessing membrane material properties from the response of giant unilamellar vesicles to electric fields”. *Advances in Physics: X* 8.1 (2023), #2125342. https://doi.org/10.1080/23746149.2022.2125342.

[6] E. Amstad, J. Kohlbrecher, E. Müller, T. Schweizer, M. Textor, and E. Reimhult. “Triggered Release from Liposomes through Magnetic Actuation of Iron Oxide Nanoparticle Containing Membranes”. *Nano Letters* 11.4 (2011), pp. 1664–1670. https://doi.org/10.1021/nl2001499.

[7] V. V. S. N. L. Andra, S. V. N. Pammi, L. V. K. P. Bhatraju, and L. K. Ruddaraju. “A Comprehensive Review on Novel Liposomal Methodologies, Commercial Formulations, Clinical Trials and Patents”. *BioNanoScience* 12 (2022), pp. 274–291. https://doi.org/10.1007/s12668-022-00941-x.

[8] C. Årdal, E. Baraldi, U. Theuretzbacher, K. Outterson, J. Plahte, F. Ciabuschi, and J.-A. Røttingen. “Insights into early stage of antibiotic development in small- and medium-sized enterprises: a survey of targets, costs, and durations”. *Journal of Pharmaceutical Policy and Practice* 11.1 (2018), p. 8. https://doi.org/10.1186/s40545-018-0135-0.

[9] K. J. Åström and R. M. Murray. *Feedback Systems: An Introduction for Scientists and Engineers*. Version v2.10c. Princeton University Press, 2008. https://doi.org/10.2307/j.ctvcm4gdk.

[10] A. Atay, A. Topuz, B. Sarıarslan, E. Yıldırım, J. Charmet, K. Couling, and B. Çetin. “Flow rate-controlled pipetting for microfluidics: second-generation flexible hydraulic reservoir (FHRv2)”. *Microfluidics and Nanofluidics* 25 (2021), #3. https://doi.org/10.1007/s10404-020-02402-x.

[11] Y. H. Bae and K. Park. “Targeted drug delivery to tumors: Myths, reality and possibility”. *Journal of Controlled Release* 153.3 (2011), pp. 198–205. https://doi.org/10.1016/j.jconrel.2011.06.001.

[12] A. Bakhtiari and C. J. Kähler. “A method to prevent clogging and clustering in microfluidic systems using microbubble streaming”. *Biomicrofluidics* 18.4 (2024), #044101. https://doi.org/10.1063/5.0214436.

[13] A. D. Bangham, M. M. Standish, and J. C. Watkins. “Diffusion of univalent ions across the lamellae of swollen phospholipids”. *Journal of Molecular Biology* 13.1 (1965), pp. 238–252, IN26–IN27. https://doi.org/10.1016/S0022-2836(65)80093-6.

[14] Y. Barenholz. “Doxil® — The first FDA-approved nano-drug: Lessons learned”. *Journal of Controlled Release*. Past, current and future applications of liposomes - Grand Challenges and Opportunities in Nanomedicine 160.2 (2012), pp. 117–134. https://doi.org/10.1016/j.jconrel.2012.03.020.

[15] S. Bartkova, M. Vendelin, I. Sanka, P. Pata, and O. Scheler. “Droplet image analysis with user-friendly freeware CellProfiler”. *Analytical Methods* 12.17 (2020), pp. 2287–2294. https://doi.org/10.1039/D0AY00031K.

[16] S. Batzri and E. D. Korn. “Single bilayer liposomes prepared without sonication”. *Biochimica et Biophysica Acta (BBA) - Biomembranes* 298.4 (1973), pp. 1015–1019. https://doi.org/10.1016/0005-2736(73)90408-2.

[17] A. Beck, L. Goetsch, C. Dumontet, and N. Corvaïa. “Strategies and challenges for the next generation of antibody–drug conjugates”. *Nature Reviews Drug Discovery* 16.5 (2017), pp. 315–337. https://doi.org/10.1038/nrd.2016.268.

[18] M. R. Behrens, H. C. Fuller, E. R. Swist, J. Wu, M. M. Islam, Z. Long, W. C. Ruder, and R. Steward. “Open-source, 3D-printed Peristaltic Pumps for Small Volume Point-of-Care Liquid Handling”. *Scientific Reports* 10 (2020), #1543. https://doi.org/10.1038/s41598-020-58246-6.

[19] J. M. Berg, J. L. Tymoczko, and L. Stryer. *Biochemistry, Fifth Edition: International Version*. New York: W. H. Freeman, 2003.

[20] N. Berger, A. Sachse, J. Bender, R. Schubert, and M. Brandl. “Filter extrusion of liposomes using different devices: comparison of liposome size, encapsulation efficiency, and process characteristics”. *International Journal of Pharmaceutics* 223.1 (2001), pp. 55–68. https://doi.org/10.1016/S0378-5173(01)00721-9.

[21] R. P. Borase, D. K. Maghade, S. Y. Sondkar, and S. N. Pawar. “A review of PID control, tuning methods and applications”. *International Journal of Dynamics and Control* 9.2 (2021), pp. 818–827. https://doi.org/10.1007/s40435-020-00665-4.

[22] F. Bray, M. Laversanne, H. Sung, J. Ferlay, R. L. Siegel, I. Soerjomataram, and A. Jemal. “Global cancer statistics 2022: GLOBOCAN estimates of incidence and mortality worldwide for 36 cancers in 185 countries”. *CA: A Cancer Journal for Clinicians* 74.3 (2024), pp. 229–263. https://doi.org/10.3322/caac.21834.

[23] J. T. Buboltz and G. W. Feigenson. “A novel strategy for the preparation of liposomes: rapid solvent exchange”. *Biochimica et Biophysica Acta (BBA) - Biomembranes* 1417.2 (1999), pp. 232–245. https://doi.org/10.1016/S0005-2736(99)00006-1.

[24] C. K. Byun, K. Abi-Samra, Y.-K. Cho, and S. Takayama. “Pumps for microfluidic cell culture”. *Electrophoresis* 35.2-3 (2014), pp. 245–257. https://doi.org/10.1002/elps.201300205.

[25] R. P. Carney, R. R. Mizenko, B. T. Bozkurt, N. Lowe, T. Henson, A. Arizzi, A. Wang, C. Tan, and S. C. George. “Harnessing extracellular vesicle heterogeneity for diagnostic and therapeutic applications”. *Nature Nanotechnology* 20.1 (2025), pp. 14–25. https://doi.org/10.1038/s41565-024-01774-3.

[26] *CAS Common Chemistry*. URL: https://commonchemistry.cas.org/detail?cas_rn=26853-31-6 (visited on 02/02/2026).

[27] X. Cong, J. Chen, and R. Xu. “Recent Progress in Bio-Responsive Drug Delivery Systems for Tumor Therapy”. *Frontiers in Bioengineering and Biotechnology* 10 (2022), #916952. https://doi.org/10.3389/fbioe.2022.916952.

[28] Y. Couch, E. I. Buzàs, D. D. Vizio, Y. S. Gho, P. Harrison, A. F. Hill, J. Lötvall, G. Raposo, P. D. Stahl, C. Théry, K. W. Witwer, and D. R. F. Carter. “A brief history of nearly EV-erything – The rise and rise of extracellular vesicles”. *Journal of Extracellular Vesicles* 10.14 (2021), e12144. https://doi.org/10.1002/jev2.12144.

[29] A. Csiszár, N. Hersch, S. Dieluweit, R. Biehl, R. Merkel, and B. Hoffmann. “Novel Fusogenic Liposomes for Fluorescent Cell Labeling and Membrane Modification”. *Bioconjugate Chemistry* 21.3 (2010), pp. 537–543. https://doi.org/10.1021/bc900470y.

[30] T. Czerniak and J. P. Saenz. “Effects of lipid membranes on RNA catalytic activity and stability”. *Biology of the Cell* 117.2 (2025), e202400115. https://doi.org/10.1111/boc.202400115.

[31] S. Deshpande, Y. Caspi, A. E. C. Meijering, and C. Dekker. “Octanol-assisted liposome assembly on chip”. *Nature Communications* 7 (2016), #10447. https://doi.org/10.1038/ncomms10447.

[32] M. Di Muzio, R. Millan-Solsona, A. Dols-Perez, J. H. Borrell, L. Fumagalli, and G. Gomila. “Dielectric properties and lamellarity of single liposomes measured by in-liquid scanning dielectric microscopy”. *Journal of Nanobiotechnology* 19 (2021), #167. https://doi.org/10.1186/s12951-021-00912-6.

[33] E. Dressaire and A. Sauret. “Clogging of microfluidic systems”. *Soft Matter* 13.1 (2017), pp. 37–48. https://doi.org/10.1039/C6SM01879C.

[34] R. F. Egerton and M. Watanabe. “Spatial resolution in transmission electron microscopy”. *Micron* 160 (2022), #103304. https://doi.org/10.1016/j.micron.2022.103304.

[35] T. Eklund, C. M. Tonauer, F. Lehmkühler, and K. Amann-Winkel. “Global q-Dependent Inverse Transforms of Intensity Autocorrelation Data”. *Photon Science* (2025). https://doi.org/10.1021/photonsci.5c00014.

[36] A. Ettinger and T. Wittmann. “Chapter 5 – Fluorescence live cell imaging”. *Methods in Cell Biology*. Ed. by J. C. Waters and T. Wittman. Vol. 123. Quantitative Imaging in Cell Biology. Academic Press, 2014, pp. 77–94. https://doi.org/10.1016/B978-0-12-420138-5.00005-7.

[37] M. Faivre, C. Renoux, A. Bessaa, L. Da Costa, P. Joly, A. Gauthier, and P. Connes. “Mechanical Signature of Red Blood Cells Flowing Out of a Microfluidic Constriction Is Impacted by Membrane Elasticity, Cell Surface-to-Volume Ratio and Diseases”. *Frontiers in Physiology* 11 (2020), #576. https://doi.org/10.3389/fphys.2020.00576.

[38] S. F. Fenz and K. Sengupta. “Giant vesicles as cell models”. *Integrative Biology* 4.9 (2012), pp. 982–995. https://doi.org/10.1039/c2ib00188h.

[39] N. A. Filatov, A. A. Evstrapov, and A. S. Bukatin. “Negative Pressure Provides Simple and Stable Droplet Generation in a Flow-Focusing Microfluidic Device”. *Micromachines* 12.6 (2021), #662. https://doi.org/10.3390/mi12060662.

[40] L. E. Franken, K. Grünewald, E. J. Boekema, and M. C. A. Stuart. “A Technical Introduction to Transmission Electron Microscopy for Soft-Matter: Imaging, Possibilities, Choices, and Technical Developments”. *Small* 16.14 (2020), #1906198. https://doi.org/10.1002/smll.201906198.

[41] B. J. Frisken. “Revisiting the method of cumulants for the analysis of dynamic light-scattering data”. *Applied Optics* 40.24 (2001), pp. 4087–4091. https://doi.org/10.1364/AO.40.004087.

[42] Y. Fu and W. J. Kao. “Drug Release Kinetics and Transport Mechanisms of Non-degradable and Degradable Polymeric Delivery Systems”. *Expert Opinion on Drug Delivery* 7.4 (2010), pp. 429–444. https://doi.org/10.1517/17425241003602259.

[43] N. Fukutake. “A general theory of far-field optical microscopy image formation and resolution limit using double-sided Feynman diagrams”. *Scientific Reports* 10 (2020), #17644. https://doi.org/10.1038/s41598-020-73584-1.

[44] R. Z. Gao, M. Hébert, J. Huissoon, and C. L. Ren. “µPump: An open-source pressure pump for precision fluid handling in microfluidics”. *HardwareX* 7 (2020), e00096. https://doi.org/10.1016/j.ohx.2020.e00096.

[45] S. C. Gasoto, B. J. Schneider, and J. A. P. Setti. “Study of the Pulse of Peristaltic Pumps for Use in 3D Extrusion Bioprinting”. *ACS Omega* 7.28 (2022), pp. 24091–24101. https://doi.org/10.1021/acsomega.1c07093.

[46] *GESTIS-Stoffdatenbank*. URL: https://gestis.dguv.de/data?name=037840&lang=en (visited on 01/27/2026).

[47] T. Goršak, M. Drab, D. Križaj, M. Jeran, J. Genova, S. Kralj, D. Lisjak, V. Kralj-Iglič, A. Iglič, and D. Makovec. “Magneto-mechanical actuation of barium-hexaferrite nanoplatelets for the disruption of phospholipid membranes”. *Journal of Colloid and Interface Science* 579 (2020), pp. 508–519. https://doi.org/10.1016/j.jcis.2020.06.079.

[48] M. N. S. de Graaf, A. Vivas, A. D. van der Meer, C. L. Mummery, and V. V. Orlova. “Pressure-Driven Perfusion System to Control, Multiplex and Recirculate Cell Culture Medium for Organs-on-Chips”. *Micromachines* 13.8 (2022), #1359. https://doi.org/10.3390/mi13081359.

[49] K. Grindulis, N. G. Matusevica, V. Kozlova, R. Rimsa, K. Klavins, and G. Mozolevskis. “Sorption and release of small molecules in PDMS and COC for Organs on chip”. *Scientific Reports* 15 (2025), #14012. https://doi.org/10.1038/s41598-025-97111-2.

[50] A. Groisman, C. Lobo, H. Cho, J. K. Campbell, Y. S. Dufour, A. M. Stevens, and A. Levchenko. “A microfluidic chemostat for experiments with bacterial and yeast cells”. *Nature Methods* 2.9 (2005), pp. 685–689. https://doi.org/10.1038/nmeth784.

[51] H. Guo, W. Chen, X. Sun, Y.-N. Liu, J. Li, and J. Wang. “Theranostic magnetoliposomes coated by carboxymethyl dextran with controlled release by low-frequency alternating magnetic field”. *Carbohydrate Polymers* 118 (2015), pp. 209–217. https://doi.org/10.1016/j.carbpol.2014.10.076.

[52] S. Habet. “Narrow Therapeutic Index drugs: clinical pharmacology perspective”. *Journal of Pharmacy and Pharmacology* 73.10 (2021), pp. 1285–1291. https://doi.org/10.1093/jpp/rgab102.

[53] A. R. Halpern, M. Y. Lee, M. D. Howard, M. A. Woodworth, P. R. Nicovich, and J. C. Vaughan. “Versatile, do-it-yourself, low-cost spinning disk confocal microscope”. *Biomedical Optics Express* 13.2 (2022), pp. 1102–1120. https://doi.org/10.1364/BOE.442087.

[54] S. Hamann, J. F. Kiilgaard, T. Litman, F. J. Alvarez-Leefmans, B. R. Winther, and T. Zeuthen. “Measurement of Cell Volume Changes by Fluorescence Self-Quenching”. *Journal of Fluorescence* 12.2 (2002), pp. 139–145. https://doi.org/10.1023/A:1016832027325.

[55] M. E. Haque, A. Matin, X. Wang, and M. Kersaudy-Kerhoas. “Effects of syringe pump fluctuations on cell-free layer in hydrodynamic separation microfluidic devices”. *Physics of Fluids* 33.7 (2021), #073317. https://doi.org/10.1063/5.0057415.

[56] L. A. Hargett and N. N. Bauer. “On the origin of microparticles: From “platelet dust” to mediators of intercellular communication”. *Pulmonary Circulation* 3.2 (2013), pp. 329–340. https://doi.org/10.4103/2045-8932.114760.

[57] M. Hébert, W. Baxter, J. P. Huissoon, and C. L. Ren. “A Quantitative study of the dynamic response of soft tubing for pressure-driven flow in a microfluidics context”. *Microfluidics and Nanofluidics* 24.12 (2020), #90. https://doi.org/10.1007/s10404-020-02396-6.

[58] L. Hines, K. Petersen, G. Z. Lum, and M. Sitti. “Soft Actuators for Small-Scale Robotics”. *Advanced Materials* 29.13 (2017), #1603483. https://doi.org/10.1002/adma.201603483.

[59] P. van Hoogevest and A. Wendel. “The use of natural and synthetic phospholipids as pharmaceutical excipients”. *European Journal of Lipid Science and Technology* 116.9 (2014), pp. 1088–1107. https://doi.org/10.1002/ejlt.201400219.

[60] J. M. Hughes, P. M. Budd, A. Grieve, P. Dutta, K. Tiede, and J. Lewis. “Highly monodisperse, lanthanide-containing polystyrene nanoparticles as potential standard reference materials for environmental “nano” fate analysis”. *Journal of Applied Polymer Science* 132.24 (2015), #42061. https://doi.org/10.1002/app.42061.

[61] D. Huh, B. D. Matthews, A. Mammoto, M. Montoya-Zavala, H. Y. Hsin, and D. E. Ingber. “Reconstituting Organ-Level Lung Functions on a Chip”. *Science* 328.5986 (2010), pp. 1662–1668. https://doi.org/10.1126/science.1188302.

[62] J. Hyeon and H. So. “Microfabricaton of microfluidic check valves using comb-shaped moving plug for suppression of backflow in microchannel”. *Biomedical Microdevices* 21 (2019), #19. https://doi.org/10.1007/s10544-019-0365-1.

[63] D. E. Ingber. “Human organs-on-chips for disease modelling, drug development and personalized medicine”. *Nature Reviews Genetics* 23.8 (2022), pp. 467–491. https://doi.org/10.1038/s41576-022-00466-9.

[64] A. Jalili, M. Bagheri, A. Shamloo, and A. H. Kazemipour Ashkezari. “A plasmonic gold nanofilm-based microfluidic chip for rapid and inexpensive droplet-based photonic PCR”. *Scientific Reports* 11 (2021), #23338. https://doi.org/10.1038/s41598-021-02535-1.

[65] Z. Jiao, J. Zhao, Z. Chao, Z. You, and J. Zhao. “An air-chamber-based microfluidic stabilizer for attenuating syringe-pump-induced fluctuations”. *Microfluidics and Nanofluidics* 23.2 (2019), #26. https://doi.org/10.1007/s10404-019-2193-2.

[66] H. Kanniyappan, J. Jose, S. Chakraborty, M. Ramasamy, and V. Muthuvijayan. “pH-responsive drug release from positively charged mesoporous silica nanoparticles and their potential for anticancer drug delivery”. *Journal of the Australian Ceramic Society* 59 (2023), pp. 207–220. https://doi.org/10.1007/s41779-022-00827-x.

[67] M. Kaszuba, D. McKnight, M. T. Connah, F. K. McNeil-Watson, and U. Nobbmann. “Measuring sub nanometre sizes using dynamic light scattering”. *Journal of Nanoparticle Research* 10.5 (2008), pp. 823–829. https://doi.org/10.1007/s11051-007-9317-4.

[68] H. Kato, M. Suzuki, K. Fujita, M. Horie, S. Endoh, Y. Yoshida, H. Iwahashi, K. Takahashi, A. Nakamura, and S. Kinugasa. “Reliable size determination of nanoparticles using dynamic light scattering method for in vitro toxicology assessment”. *Toxicology in Vitro* 23.5 (2009), pp. 927–934. https://doi.org/10.1016/j.tiv.2009.04.006.

[69] R. U. Khan, J. Shao, J.-Y. Liao, and L. Qian. “pH-triggered cancer-targeting polymers: From extracellular accumulation to intracellular release”. *Nano Research* 16.4 (2023), pp. 5155–5168. https://doi.org/10.1007/s12274-022-5252-z.

[70] M. R. Krause and S. L. Regen. “The Structural Role of Cholesterol in Cell Membranes: From Condensed Bilayers to Lipid Rafts”. *Accounts of Chemical Research* 47.12 (2014), pp. 3512–3521. https://doi.org/10.1021/ar500260t.

[71] S. Kube, N. Hersch, E. Naumovska, T. Gensch, J. Hendriks, A. Franzen, L. Landvogt, J.-P. Siebrasse, U. Kubitscheck, B. Hoffmann, R. Merkel, and A. Csiszár. “Fusogenic Liposomes as Nanocarriers for the Delivery of Intracellular Proteins”. *Langmuir* 33.4 (2017), pp. 1051–1059. https://doi.org/10.1021/acs.langmuir.6b04304.

[72] T. Lajunen, L.-S. Kontturi, L. Viitala, M. Manna, O. Cramariuc, T. Róg, A. Bunker, T. Laaksonen, T. Viitala, L. Murtomäki, and A. Urtti. “Indocyanine Green-Loaded Liposomes for Light-Triggered Drug Release”. *Molecular Pharmaceutics* 13.6 (2016), pp. 2095–2107. https://doi.org/10.1021/acs.molpharmaceut.6b00207.

[73] J. R. Lake, K. C. Heyde, and W. C. Ruder. “Low-cost feedback-controlled syringe pressure pumps for microfluidics applications”. *PLOS One* 12.4 (2017), e0175089. https://doi.org/10.1371/journal.pone.0175089.

[74] E. Lauga and T. R. Powers. “The hydrodynamics of swimming microorganisms”. *Reports on Progress in Physics* 72.9 (2009), #096601. https://doi.org/10.1088/0034-4885/72/9/096601.

[75] M. Laurencin, T. Georgelin, B. Malezieux, J.-M. Siaugue, and C. Ménager. "Interactions Between Giant Unilamellar Vesicles and Charged Core-Shell Magnetic Nanoparticles". *Langmuir* 26.20 (2010), pp. 16025–16030. https://doi.org/10.1021/la1023746.

[76] Y. Lee and D. Thompson. "Stimuli-responsive liposomes for drug delivery". *WIREs Nanomedicine and Nanobiotechnology* 9.5 (2017), e1450. https://doi.org/10.1002/wnan.1450.

[77] M. Leuthner and O. Hayden. "Grease the gears: how lubrication of syringe pumps impacts microfluidic flow precision". *Lab on a Chip* 24.1 (2023), pp. 56–62. https://doi.org/10.1039/D3LC00698K.

[78] J. W. Lichtman and J.-A. Conchello. "Fluorescence microscopy". *Nature Methods* 2.12 (2005), pp. 910–919. https://doi.org/10.1038/nmeth817.

[79] J. Lim, S. P. Yeap, H. X. Che, and S. C. Low. "Characterization of magnetic nanoparticle by dynamic light scattering". *Nanoscale Research Letters* 8 (2013), #381. https://doi.org/10.1186/1556-276X-8-381.

[80] J. F. Liu, N. Neel, P. Dang, M. Lamb, J. McKenna, L. Rodgers, B. Litt, Z. Cheng, A. Tsourkas, and D. Issadore. "Radiofrequency-Triggered Drug Release from Nanoliposomes with Millimeter-Scale Resolution Using a Superimposed Static Gating Field". *Small* 14.44 (2018), #1802563. https://doi.org/10.1002/smll.201802563.

[81] Y. Liu, F. Yang, C. Yuan, M. Li, T. Wang, B. Chen, J. Jin, P. Zhao, J. Tong, S. Luo, and N. Gu. "Magnetic Nanoliposomes as in Situ Microbubble Bombers for Multimodality Image-Guided Cancer Theranostics". *ACS Nano* 11.2 (2017), pp. 1509–1519. https://doi.org/10.1021/acsnano.6b06815.

[82] Y. Liu, L. Chen, Q. Shi, Q. Zhao, and H. Ma. "Tumor Microenvironment–Responsive Polypeptide Nanogels for Controlled Antitumor Drug Delivery". *Frontiers in Pharmacology* 12 (2021), #748102. https://doi.org/10.3389/fphar.2021.748102.

[83] D. Lombardo and M. A. Kiselev. "Methods of Liposomes Preparation: Formation and Control Factors of Versatile Nanocarriers for Biomedical and Nanomedicine Application". *Pharmaceutics* 14.3 (2022), #543. https://doi.org/10.3390/pharmaceutics14030543.

[84] T. Lu and T. L. M. ten Hagen. "A novel kinetic model to describe the ultra-fast triggered release of thermosensitive liposomal drug delivery systems". *Journal of Controlled Release* 324 (2020), pp. 669–678. https://doi.org/10.1016/j.jconrel.2020.05.047.

[85] M. Malamatari. "The Importance of Drug Delivery in the Clinical Development and Lifecycle of Drug Products with Examples from Authorised Medicinal Products". *Processes* 11.10 (2023), #2919. https://doi.org/10.3390/pr11102919.

[86] E. Maron, P. Krysinski, and M. Chudy. "Controlled Release of Doxorubicin from Magnetoliposomes Assisted by Low-Frequency Magnetic Field". *Chemistry & Biodiversity* 20.4 (2023), e202201079. https://doi.org/10.1002/cbdv.202201079.

[87] A. Marzouq, L. Morgenstein, C. A. Huang-Zhu, S. Yudovich, A. Atkins, A. Grupi, R. C. Van Lehn, and S. Weiss. "Long-chain lipids facilitate insertion

of large nanoparticles into membranes of small unilamellar vesicles". *Langmuir* 40.20 (2024), pp. 10477–10485. https://doi.org/10.1021/acs.langmuir.3c03471.

[88] *Microfluidic Flow Control System - Fluigent*. URL: https://www.fluigent.com/research/instruments/pressure-flow-controllers/mfcs-series/ (visited on 02/19/2025).

[89] C. A. Monnier, D. Burnand, B. Rothen-Rutishauser, M. Lattuada, and A. Petri-Fink. "Magnetoliposomes: opportunities and challenges". *European Journal of Nanomedicine* 6.4 (2014), pp. 201–215. https://doi.org/10.1515/ejnm-2014-0042.

[90] J. W. Mouton, J. Meletiadis, A. Voss, and J. Turnidge. "Variation of MIC measurements: the contribution of strain and laboratory variability to measurement precision". *Journal of Antimicrobial Chemotherapy* 73.9 (2018), pp. 2374–2379. https://doi.org/10.1093/jac/dky232.

[91] G. Murtas, Y. Kuruma, P. Bianchini, A. Diaspro, and P. L. Luisi. "Protein synthesis in liposomes with a minimal set of enzymes". *Biochemical and Biophysical Research Communications* 363.1 (2007), pp. 12–17. https://doi.org/10.1016/j.bbrc.2007.07.201.

[92] M. Naiim, A. Boualem, C. Ferre, M. Jabloun, A. Jalocha, and P. Ravier. "Multiangle dynamic light scattering for the improvement of multimodal particle size distribution measurements". *Soft Matter* 11.1 (2015), pp. 28–32. https://doi.org/10.1039/C4SM01995D.

[93] M. Najah, A. D. Griffiths, and M. Ryckelynck. "Teaching Single-Cell Digital Analysis Using Droplet-Based Microfluidics". *Analytical Chemistry* 84.3 (2012), pp. 1202–1209. https://doi.org/10.1021/ac202645m.

[94] S. Nappini, M. Bonini, F. B. Bombelli, F. Pineider, C. Sangregorio, P. Baglioni, and B. Nordèn. "Controlled drug release under a low frequency magnetic field: effect of the citrate coating on magnetoliposomes stability". *Soft Matter* 7.3 (2011), pp. 1025–1037. https://doi.org/10.1039/C0SM00789G.

[95] S. Nappini, M. Bonini, F. Ridi, and P. Baglioni. "Structure and permeability of magnetoliposomes loaded with hydrophobic magnetic nanoparticles in the presence of a low frequency magnetic field". *Soft Matter* 7.10 (2011), pp. 4801–4811. https://doi.org/10.1039/C0SM01264E.

[96] V. Narayanamurthy, Z. E. Jeroish, K. S. Bhuvaneshwari, P. Bayat, R. Premkumar, F. Samsuri, and M. M. Yusoff. "Advances in passively driven microfluidics and lab-on-chip devices: a comprehensive literature review and patent analysis". *RSC Advances* 10.20 (2020), pp. 11652–11680. https://doi.org/10.1039/D0RA00263A.

[97] W. Nauwynck, K. Faust, and N. Boon. "Droplet microfluidics for single-cell studies: a frontier in ecological understanding of microbiomes". *FEMS Microbiology Reviews* 49 (2025), fuaf032. https://doi.org/10.1093/femsre/fuaf032.

[98] A.-G. Niculescu, C. Chircov, A. C. Bîrcă, and A. M. Grumezescu. "Fabrication and Applications of Microfluidic Devices: A Review". *International Journal of Molecular Sciences* 22.4 (2021), #2011. https://doi.org/10.3390/ijms22042011.

[99] R. Ning, B. Acree, M. Wu, and Y. Gao. “Microfluidic Monodispersed Microbubble Generation for Production of Cavitation Nuclei”. *Micromachines* 15.12 (2024), #1531. https://doi.org/10.3390/mi15121531.

[100] J. M. Nitsche and G. B. Kasting. “A Universal Correlation Predicts Permeability Coefficients of Fluid- and Gel-Phase Phospholipid and Phospholipid-Cholesterol Bilayers for Arbitrary Solutes”. *Journal of Pharmaceutical Sciences* 105.5 (2016), pp. 1762–1771. https://doi.org/10.1016/j.xphs.2016.02.012.

[101] T. Niwa, Y. Sasaki, E. Uemura, S. Nakamura, M. Akiyama, M. Ando, S. Sawada, S.-a. Mukai, T. Ueda, H. Taguchi, and K. Akiyoshi. “Comprehensive study of liposome-assisted synthesis of membrane proteins using a reconstituted cell-free translation system”. *Scientific Reports* 5 (2015), #18025. https://doi.org/10.1038/srep18025.

[102] A. Nwaneshiudu, C. Kuschal, F. H. Sakamoto, R. R. Anderson, K. Schwarzenberger, and R. C. Young. “Introduction to Confocal Microscopy”. *Journal of Investigative Dermatology* 132.12 (2012), pp. 1–5. https://doi.org/10.1038/jid.2012.429.

[103] *OB1 MK4 Flow controller*. URL: https://www.elveflow.com/microfluidic-products/microfluidics-flow-control-systems/ob1-pressure-controller/ (visited on 02/19/2025).

[104] K. W. Oh, K. Lee, B. Ahn, and E. P. Furlani. “Design of pressure-driven microfluidic networks using electric circuit analogy”. *Lab on a Chip* 12.3 (2012), pp. 515–545. https://doi.org/10.1039/C2LC20799K.

[105] S. G. M. Ong, M. Chitneni, K. S. Lee, L. C. Ming, and K. H. Yuen. “Evaluation of Extrusion Technique for Nanosizing Liposomes”. *Pharmaceutics* 8.4 (2016), #36. https://doi.org/10.3390/pharmaceutics8040036.

[106] F. Ott, T. Meyer-Zedler, M. Schmitt, and J. Popp. “Image-based fuzzy logic control for pressure-driven droplet microfluidics as autosampler for multimodal imaging microscopy”. *Lab on a Chip* 25.2 (2025), pp. 119–126. https://doi.org/10.1039/D4LC00583J.

[107] H. Parhiz, M. Khoshnejad, J. W. Myerson, E. Hood, P. N. Patel, J. S. Brenner, and V. R. Muzykantov. “Unintended effects of drug carriers: big issues of small particles”. *Advanced drug delivery reviews* 130 (2018), pp. 90–112. https://doi.org/10.1016/j.addr.2018.06.023.

[108] P. A. Penczek. “Resolution measures in molecular electron microscopy”. *Methods in enzymology* 482 (2010), pp. 73–100. https://doi.org/10.1016/S0076-6879(10)82003-8.

[109] D. A. Pereira, A. D. Silva, P. A. T. Martins, A. P. Piedade, D. Martynowych, D. Veysset, M. J. Moreno, C. Serpa, K. A. Nelson, and L. G. Arnaut. “Imaging of photoacoustic-mediated permeabilization of giant unilamellar vesicles (GUVs)”. *Scientific Reports* 11 (2021), #2775. https://doi.org/10.1038/s41598-021-82140-4.

[110] R. Pichot, R. L. Watson, and I. T. Norton. “Phospholipids at the Interface: Current Trends and Challenges”. *International Journal of Molecular Sciences* 14.6 (2013), pp. 11767–11794. https://doi.org/10.3390/ijms140611767.

[111] J. H. Pollard and E. J. Valkovics. “The Gompertz Distribution and Its Applications”. *Genus* 48.3/4 (1992), pp. 15–28. URL: https://www.jstor.org/stable/29789100 (visited on 01/23/2026).

[112] C. Quintard, E. Tubbs, G. Jonsson, J. Jiao, J. Wang, N. Werschler, C. Laporte, A. Pitaval, T.-S. Bah, G. Pomeranz, C. Bissardon, J. Kaal, A. Leopoldi, D. A. Long, P. Blandin, J.-L. Achard, C. Battail, A. Hagelkruys, F. Navarro, Y. Fouillet, J. M. Penninger, and X. Gidrol. "A microfluidic platform integrating functional vascularized organoids-on-chip". *Nature Communications* 15 (2024), #1452. https://doi.org/10.1038/s41467-024-45710-4.

[113] O. Reinsalu, M. Ernits, and V. Linko. "Liposome-based hybrid drug delivery systems with DNA nanostructures and metallic nanoparticles". *Expert Opinion on Drug Delivery* 21.6 (2024), pp. 905–920. https://doi.org/10.1080/17425247.2024.2375389.

[114] O. Reinsalu, A. Samel, E. Niemeister, and R. Kurg. "MAGEA4 Coated Extracellular Vesicles Are Stable and Can Be Assembled In Vitro". *International Journal of Molecular Sciences* 22.10 (2021), #5208. https://doi.org/10.3390/ijms22105208.

[115] E. Rideau, R. Dimova, P. Schwille, F. R. Wurm, and K. Landfester. "Liposomes and polymersomes: a comparative review towards cell mimicking". *Chemical Society Reviews* 47.23 (2018), pp. 8572–8610. https://doi.org/10.1039/C8CS00162F.

[116] J. Risbo, K. Jørgensen, M. M. Sperotto, and O. G. Mouritsen. "Phase behavior and permeability properties of phospholipid bilayers containing a short-chain phospholipid permeability enhancer". *Biochimica et Biophysica Acta (BBA) - Biomembranes* 1329.1 (1997), pp. 85–96. https://doi.org/10.1016/S0005-2736(97)00091-6.

[117] A.-L. Robson, P. C. Dastoor, J. Flynn, W. Palmer, A. Martin, D. W. Smith, A. Woldu, and S. Hua. "Advantages and Limitations of Current Imaging Techniques for Characterizing Liposome Morphology". *Frontiers in Pharmacology* 9 (2018), #80. https://doi.org/10.3389/fphar.2018.00080.

[118] D. Romanini, M. Di Martino, L. Sessa, S. Concilio, and S. Piotto. "Electroformation of Giant Unilamellar vesicles: Novel electrode design and parameters for enhanced GUVs production". *Bioelectrochemistry* 169 (2026), #109192. https://doi.org/10.1016/j.bioelechem.2025.109192.

[119] J. Saez, R. Catalan-Carrio, R. M. Owens, L. Basabe-Desmonts, and F. Benito-Lopez. "Microfluidics and materials for smart water monitoring: A review". *Analytica Chimica Acta* 1186 (2021), #338392. https://doi.org/10.1016/j.aca.2021.338392.

[120] H. S. Sanchez and C. B. Chang. "Open-source pneumatic pressure pump for drop-based microfluidic flow controls". *Engineering Research Express* 5.3 (2023), #035014. https://doi.org/10.1088/2631-8695/ace299.

[121] I. Sanka, S. Bartkova, P. Pata, O.-P. Smolander, and O. Scheler. "Investigation of Different Free Image Analysis Software for High-Throughput Droplet Detection". *ACS Omega* 6.35 (2021), pp. 22625–22634. https://doi.org/10.1021/acsomega.1c02664.

[122] F. b. N. Sarbaland, M. Kobayashi, D. Tanaka, R. Fujita, N. Tanaka, and M. Furuya. "Temperature Control in Microfluidic Devices: Approaches, Challenges, and Future Directions". *Applied Sciences* 15.18 (2025), #9902. https://doi.org/10.3390/app15189902.

[123] O. Scheler, K. Makuch, P. R. Debski, M. Horka, A. Ruszczak, N. Pacocha, K. Sozański, O.-P. Smolander, W. Postek, and P. Garstecki. "Droplet-based digital

antibiotic susceptibility screen reveals single-cell clonal heteroresistance in an isogenic bacterial population". *Scientific Reports* 10 (2020), #3282. https://doi.org/10.1038/s41598-020-60381-z.

[124] J. Schmitz, B. Stute, S. Täuber, D. Kohlheyer, E. von Lieres, and A. Grünberger. "Reliable cell retention of mammalian suspension cells in microfluidic cultivation chambers". *Scientific Reports* 13 (2023), #3857. https://doi.org/10.1038/s41598-023-30297-5.

[125] O. A. Solis-Gonzalez, J. R. Avendaño-Gómez, and A. Rojas-Aguilar. "A thermodynamic study of F108 and F127 block copolymer interactions with liposomes at physiological temperature". *Journal of Liposome Research* 32.1 (2022), pp. 32–44. https://doi.org/10.1080/08982104.2020.1865401.

[126] T. M. Squires and S. R. Quake. "Microfluidics: Fluid physics at the nanoliter scale". *Reviews of Modern Physics* 77.3 (2005), pp. 977–1026. https://doi.org/10.1103/RevModPhys.77.977.

[127] B. Srinivasan and M. D. Lloyd. "Dose–Response Curves and the Determination of IC50 and EC50 Values". *Journal of Medicinal Chemistry* 67.20 (2024), pp. 17931–17934. https://doi.org/10.1021/acs.jmedchem.4c02052.

[128] N. R. H. Stone, T. Bicanic, R. Salim, and W. Hope. "Liposomal Amphotericin B (AmBisome®): A Review of the Pharmacokinetics, Pharmacodynamics, Clinical Experience and Future Directions". *Drugs* 76.4 (2016), pp. 485–500. https://doi.org/10.1007/s40265-016-0538-7.

[129] K. Strebhardt and A. Ullrich. "Paul Ehrlich's magic bullet concept: 100 years of progress". *Nature Reviews Cancer* 8.6 (2008), pp. 473–480. https://doi.org/10.1038/nrc2394.

[130] J. Sudimack and R. J. Lee. "Targeted drug delivery via the folate receptor". *Advanced Drug Delivery Reviews*. Recent Advances in Cellular, Subcellular and Molecular Targeting 41.2 (2000), pp. 147–162. https://doi.org/10.1016/S0169-409X(99)00062-9.

[131] H. Talsma, A. Y. Özer, L. v. Bloois, and D. J. A. Crommelin. "The Size Reduction of Liposomes with a High Pressure Homogenizer (Microfluidizer™). Characterization of Prepared Dispersions and Comparison with Conventional Methods." *Drug Development and Industrial Pharmacy* 15.2 (1989), pp. 197–207. https://doi.org/10.3109/03639048909040205.

[132] J. Tamargo, J.-Y. Le Heuzey, and P. Mabo. "Narrow therapeutic index drugs: a clinical pharmacological consideration to flecainide". *European Journal of Clinical Pharmacology* 71.5 (2015), pp. 549–567. https://doi.org/10.1007/s00228-015-1832-0.

[133] Y. Tamba and M. Yamazaki. "Single Giant Unilamellar Vesicle Method Reveals Effect of Antimicrobial Peptide Magainin 2 on Membrane Permeability". *Biochemistry* 44.48 (2005), pp. 15823–15833. https://doi.org/10.1021/bi051684w.

[134] P. K. Tarafdar, H. Chakraborty, S. M. Dennison, and B. R. Lentz. "Phosphatidylserine Inhibits and Calcium Promotes Model Membrane Fusion". *Biophysical Journal* 103.9 (2012), pp. 1880–1889. https://doi.org/10.1016/j.bpj.2012.09.030.

[135] R. Tenchov, R. Bird, A. E. Curtze, and Q. Zhou. "Lipid Nanoparticles–From Liposomes to mRNA Vaccine Delivery, a Landscape of Research Diversity and

Advancement". *ACS Nano* 15.11 (2021), pp. 16982–17015. https://doi.org/10.1021/acsnano.1c04996.

[136] R. Tenchov, J. M. Sasso, and Q. A. Zhou. "PEGylated Lipid Nanoparticle Formulations: Immunological Safety and Efficiency Perspective". *Bioconjugate Chemistry* 34.6 (2023), pp. 941–960. https://doi.org/10.1021/acs.bioconjchem.3c00174.

[137] A. Tewabe, A. Abate, M. Tamrie, A. Seyfu, and E. Abdela Siraj. "Targeted Drug Delivery - From Magic Bullet to Nanomedicine: Principles, Challenges, and Future Perspectives". *Journal of Multidisciplinary Healthcare* 14 (2021), pp. 1711–1724. https://doi.org/10.2147/jmdh.s313968.

[138] K. M. C. Tjørve and E. Tjørve. "The use of Gompertz models in growth analyses, and new Gompertz-model approach: An addition to the Unified-Richards family". *PLOS One* 12.6 (2017), e0178691. https://doi.org/10.1371/journal.pone.0178691.

[139] M. W. Toepke and D. J. Beebe. "PDMS absorption of small molecules and consequences in microfluidic applications". *Lab on a Chip* 6.12 (2006), pp. 1484–1486. https://doi.org/10.1039/B612140C.

[140] P. Trucillo, R. Campardelli, and E. Reverchon. "Liposomes: From Bangham to Supercritical Fluids". *Processes* 8.9 (2020), #1022. https://doi.org/10.3390/pr8091022.

[141] J. Vangindertael, R. Camacho, W. Sempels, H. Mizuno, P. Dedecker, and K. P. F. Janssen. "An introduction to optical super-resolution microscopy for the adventurous biologist". *Methods and Applications in Fluorescence* 6.2 (2018), #022003. https://doi.org/10.1088/2050-6120/aaae0c.

[142] D. B. Vieira and L. F. Gamarra. "Getting into the brain: liposome-based strategies for effective drug delivery across the blood–brain barrier". *International Journal of Nanomedicine* 11 (2016), pp. 5381–5414. https://doi.org/10.2147/IJN.S117210.

[143] K. Y. Vlasova, A. Piroyan, I. M. Le-Deygen, H. M. Vishwasrao, J. D. Ramsey, N. L. Klyachko, Y. I. Golovin, P. G. Rudakovskaya, I. I. Kireev, A. V. Kabanov, and M. Sokolsky-Papkov. "Magnetic liposome design for drug release systems responsive to super-low frequency alternating current magnetic field (AC MF)". *Journal of Colloid and Interface Science* 552 (2019), pp. 689–700. https://doi.org/10.1016/j.jcis.2019.05.071.

[144] A. R. Vollertsen, D. de Boer, S. Dekker, B. a. M. Wesselink, R. Haverkate, H. S. Rho, R. J. Boom, M. Skolimowski, M. Blom, R. Passier, A. van den Berg, A. D. van der Meer, and M. Odijk. "Modular operation of microfluidic chips for highly parallelized cell culture and liquid dosing via a fluidic circuit board". *Microsystems & Nanoengineering* 6 (2020), #107. https://doi.org/10.1038/s41378-020-00216-z.

[145] A. Wagner, K. Vorauer-Uhl, and H. Katinger. "Liposomes produced in a pilot scale: production, purification and efficiency aspects". *European Journal of Pharmaceutics and Biopharmaceutics* 54.2 (2002), pp. 213–219. https://doi.org/10.1016/S0939-6411(02)00062-0.

[146] C. Wang, T. Zhao, W. Cheng, Z. Ni, and N. Xiang. "Microfluidic strategies in soft robotics: Actuators, control systems, and pumps". *Device* 2.9 (2024), #100551. https://doi.org/10.1016/j.device.2024.100551.

[147] J. D. Wang, N. J. Douville, S. Takayama, and M. ElSayed. “Quantitative Analysis of Molecular Absorption into PDMS Microfluidic Channels”. *Annals of Biomedical Engineering* 40.9 (2012), pp. 1862–1873. https://doi.org/10.1007/s10439-012-0562-z.

[148] S. Wang, B. Li, D. McLeod, and Z. Li. “A handheld plug-and-play microfluidic liquid handling automation platform for immunoassays”. *HardwareX* 14 (2023), e00420. https://doi.org/10.1016/j.ohx.2023.e00420.

[149] A. R. Wheeler, W. R. Throndset, R. J. Whelan, A. M. Leach, R. N. Zare, Y. H. Liao, K. Farrell, I. D. Manger, and A. Daridon. “Microfluidic Device for Single-Cell Analysis”. *Analytical Chemistry* 75.14 (2003), pp. 3581–3586. https://doi.org/10.1021/ac0340758.

[150] J. Wildfire, N. Waterlow, A. Clements, N. Fuller, and G. Knight. “MIC distribution analysis identifies differences in AMR between population sub-groups”. *Wellcome Open Research* 9 (2024), #244. https://doi.org/10.12688/wellcomeopenres.21269.1.

[151] P. Wolf. “The Nature and Significance of Platelet Products in Human Plasma”. *British Journal of Haematology* 13.3 (1967), pp. 269–288. https://doi.org/10.1111/j.1365-2141.1967.tb08741.x.

[152] D. J. Woodbury, E. S. Richardson, A. W. Grigg, R. D. Welling, and B. H. Knudson. “Reducing Liposome Size with Ultrasound: Bimodal Size Distributions”. *Journal of Liposome Research* 16.1 (2006), pp. 57–80. https://doi.org/10.1080/08982100500528842.

[153] Y. Wu, X. Du, Y. Li, H. Tai, and Y. Su. “Optimization of temperature uniformity of a serpentine thin film heater by a two-dimensional approach”. *Microsystem Technologies* 25.1 (2019), pp. 69–82. https://doi.org/10.1007/s00542-018-3932-0.

[154] Q. Yan, Z. Liu, L. Wang, W. Sun, and M. Jiang. “Recent Research on Structural Design, Performance Optimization, and Applications of Piezoelectric Pumps”. *Micromachines* 16.4 (2025), #474. https://doi.org/10.3390/mi16040474.

[155] M. Yanagisawa, M. Iwamoto, A. Kato, K. Yoshikawa, and S. Oiki. “Oriented Reconstitution of a Membrane Protein in a Giant Unilamellar Vesicle: Experimental Verification with the Potassium Channel KcsA”. *Journal of the American Chemical Society* 133.30 (2011), pp. 11774–11779. https://doi.org/10.1021/ja2040859.

[156] N. Yandrapalli, J. Petit, O. Bäumchen, and T. Robinson. “Surfactant-free production of biomimetic giant unilamellar vesicles using PDMS-based microfluidics”. *Communications Chemistry* 4 (2021), #100. https://doi.org/10.1038/s42004-021-00530-1.

[157] A. K. Yetisen, M. S. Akram, and C. R. Lowe. “Paper-based microfluidic point-of-care diagnostic devices”. *Lab on a Chip* 13.12 (2013), pp. 2210–2251. https://doi.org/10.1039/C3LC50169H.

[158] A. P. Zbar. “In Search of the Organism and a Zauberkugeln (Magic Bullet) for Treatment*”. *Syphilis: A Short Biography*. Ed. by A. P. Zbar. Cham: Springer International Publishing, 2022, pp. 49–76. https://doi.org/10.1007/978-3-031-08968-8_4.

[159] W. Zeng, S. Li, and Z. Wang. “Characterization of syringe-pump-driven versus pressure-driven microfluidic flows”. *2015 International Conference on Fluid*

Power and Mechatronics (FPM). 2015, pp. 711–715. https://doi.org/10.1109/FPM.2015.7337207.

[160] Y. Zhai, A. Wang, D. Koh, P. Schneider, and K. W. Oh. "A robust, portable and backflow-free micromixing device based on both capillary- and vacuum-driven flows". *Lab on a Chip* 18.2 (2018), pp. 276–284. https://doi.org/10.1039/C7LC01077J.

[161] Z. Zhang, Q. Guo, Y. Wang, and H. Huang. "High-throughput screening of microbial strains in large-scale microfluidic droplets". *Frontiers in Bioengineering and Biotechnology* 11 (2023), #1105277. https://doi.org/10.3389/fbioe.2023.1105277.

[162] V. Zhemkov, J. A. Ditlev, W.-R. Lee, M. Wilson, J. Liou, M. K. Rosen, and I. Bezprozvanny. "The role of sigma 1 receptor in organization of endoplasmic reticulum signaling microdomains". *eLife* 10 (2021), e65192. https://doi.org/10.7554/eLife.65192.

[163] S. Zhen, H. XiaoMing, and L. QuanJun. "Research on Microfluidic Chip Design and Droplet Related Technology". *Journal of Physics: Conference Series* 1520 (2020), #012003. https://doi.org/10.1088/1742-6596/1520/1/012003.

[164] A. Zizzari, M. Bianco, L. Carbone, E. Perrone, F. Amato, G. Maruccio, F. Rendina, and V. Arima. "Continuous-Flow Production of Injectable Liposomes via a Microfluidic Approach". *Materials* 10.12 (2017), #1411. https://doi.org/10.3390/ma10121411.

[165] M. H. Zwietering, I. Jongenburger, F. M. Rombouts, and K. van 't Riet. "Modeling of the Bacterial Growth Curve". *Applied and Environmental Microbiology* 56.6 (1990), pp. 1875–1881. https://doi.org/10.1128/aem.56.6.1875-1881.1990.

ACKNOWLEDGMENTS

I would like to express gratitude to my supervisors Veronika Zadin, Andreas Kyritsakis, Olavi Reinsalu, and Veikko Linko, as well as the entire MATTER collective, for their guidance, support, and encouragement throughout this work. I am also sincerely thankful to Reet Kurg for valuable advice and continuous help. My thanks go to Kaido Kurrikoff for serving as the internal reviewer and for providing constructive feedback on the thesis. I am grateful to Sergei Kopantšuk and Ago Rinken for their help in gathering data for Paper I. I also thank Ott Scheler and Immanuel Sanka for discussions and for practical support in microfluidics. I wish to acknowledge Naresh Yandrapalli for insightful discussions and for providing microfluidic chips. Furthermore, I appreciate the fruitful discussions with Tatu Lajunen and Timo Laaksonen regarding liposome production. Finally, I would like to thank Jaanus Kalde for advice related to electronics and Liina Katherine Viikmaa for helping me navigate all the bureaucracy along the way.

This work was financially supported by ERA Chair MATTER from the European Union's Horizon 2020 research and innovation program under grant agreement No 856705.

Large language models were used in the writing of this thesis for language corrections and formatting.

SISUKOKKUVÕTE

Mikrovoolutuslik liposoomide valmistamine ja analüüs ruumiliselt piiritletud kaugmõjutusalaga ravimikandurite arendamiseks

Ravimite sihipärane kohaletoimetamine on teaduses olnud eesmärgiks juba üle sajandi, alates Paul Ehrlichi "võlukuuli"(ingl. k. *magic bullet)* kontseptsioonist. Tänapäeval on selleks eesmärgiks suurendada ravimi terapeutilist indeksit, hoides ära toimeainete liigset mõju tervetele kudedele. Erinevalt tavapärasest ravimite manustamisest eristatakse siin selgelt organismisisest ravimi transporti (toimetamine õigesse kohta) ja selle ohjatud vabastamist (toimeaine vabanemine juhitud kiiruse ja ajastusega). Sihitatud ravimkandur- ja ohjatud vabastamissüsteemid võimaldavad ravi tõhusust tõsta terveid kudesid puudutavate kõrvalmõjude vähendamise läbi. Toimeainete kapseldamiseks, edasikandmiseks ja vabastamiseks pakuvad häid võimalusi liposoomid. Käesoleva doktoritöö eesmärk suures plaanis oli teha samme selles suunas, et oleks võimalik välja arendada ravimkandursüsteem, mille puhul saaks kehavälisete ja mitteinvasiivsete mõjuritega ravimi toimeainet valitud kehasisestes ruumipiirkondades ravimikanduritest vabastada. Antud töös on valitud uuritavateks kanduriteks liposoomid ja konkreetseks eesmärgiks on arendada välja mikrovoolutusel ja analüütilistel meetoditel põhinev tööriistakomplekt eri suurusega liposoomide valmistamiseks ja iseloomustamiseks.

Hiiglaslikke ühekihilisi vesiikuleid (GUV, ingl. k. lüh.) valmistati mikrovoolutiga, kasutades oktanool-abistatud liposoomide koostamise (OLA, ingl. k. lüh.) meetodit. See lähenemine võimaldas vesiikulitesse täpselt kapseldada magnetilisi mikrokerasid ja fluorestsentsvalku (eGFP, ingl. k. lüh.). GUV-sid iseloomustas kitsas suurusjaotus keskmise läbimõõduga $92 \pm 6\ \mu$m. Vesiikulite püsivust ja läbilaskvust hinnates selgus, et nende arv väheneb ajas eksponentsiaalselt ja 24 h jooksul vabanes ligikaudu 90 % neisse paigutatud kaltseiinist.

Vastupidavamate kandjate saamiseks valmistati hüdrodünaamilise fokusseerimise (HDF, ingl. k. lüh.) meetodil väikeseid (SUV, ingl. k. lüh.) ja suuri (LUV, ingl. k. lüh.) ühekihilisi vesiikuleid. Dünaamilise valguse hajumise (DLS, ingl. k. lüh.) ja läbivkiirguse elektronmikroskoopia (TEM, ingl. k. lüh.) uuringud kinnitasid eri suurusega liposoomide olemasolu (umbes 80 nm, 180 nm ja 420 nm). Nanomõõdulised liposoomid olid GUV-dest märksa püsivamad: nelja päevaga väheneb osakeste hulk vaid ligi 7 % võrra, kusjuures suurusjaotuse tipud jäid endiselt 200 nm ja 430 nm juurde.

Selleks, et tagada mikrovoolutuspõhise tootmise töökindlus, valmistati nelja kanaliga piesoelektriline rõhuregulaator ja seda juhtiv tarkvarapakett. Seade võimaldab suhtelist rõhku määrata vahemikus ± 1000 mbar. Seadme raporteeritava väljundväärtuse mõõteviga jääb alla $0,7$ % ja ülemineku aeg ühelt väljundrõhult teisele on 3–10 s.

Lisaks arendati välja pildianalüüsi tarkvara nimega *EasyFlow* emulsiooni tilkade (mitsellide) ja vesiikulite uuringute andmetöötluse automatiseerimiseks. See tarkvara võimaldab objekte liigitada ja analüüsida nende polüdisperssust sobides seega suuremahuliste eksperimentide analüüsiks.

Kuigi kirjanduses esitatakse magnetoliposoomide valistamist tihti suhteliselt lihtsa protseduurina, osutus nende usaldusväärne tootmine tegelikkuses metodoloogiliselt keerukaks ülesandeks, mis ootab veel lahendamist. Üks võimalik viis selle ülesande lahendamiseks võiks olla OLA abil GUV-sid valmistades magnetilised osakesed õlifaasi (LO, ingl. k. lüh.) vedeliku kaudu membraani sisse panna. Kahjuks oleksid sellised liposoomid tõenäoliselt ikkagi oktanoolised ja liialt ebastabiilsed. Või siis oleks ka võimalik kasutada hoopis mõnda kolmandat liposoomide valmistamismeetodit, näiteks õhukese kile hüdreerimist (TFH, ingl. k. lüh.). Sellisel viisil moodustatud liposoomid oleksid HDF ja OLA meetodil toodetud liposoomidest mõõtmetelt heterogeensemad, kuid ka nende liposoomide puhul peaks olema võimalik uurida nende membraanide lekkivuse sõltuvust nende suurusest uurida. Näiteks oleks selleks võimalik kasutada liposoomide ekstruuderit, et järeltöötluses liposoomide suuruseid väiksemaks muuta ja seejärel mõõta membraanide läbistatavuse varieeruvust erinevate suurustega liposoomide puhul.

Kokkuvõttes moodustavad töös arendatud meetodid ja seadmed tervikliku süsteemi magnetiliselt tundlike liposoomsete ravimikandjate uurimiseks ja loob eeldused väliselt juhitavate toimeaine vabastamise süsteemide välja arendamiseks. Järgmine samm selles uurimussuunas on magnetoliposoomide valmistamine, milleks selles lõputöös esitatud vahendid ja meetodid loovad tugevad eeldused.

PUBLICATIONS

CURRICULUM VITAE

Personal data

Name:	Mart Ernits
Date of birth:	05.10.1989.
E-mail:	mart223@gmail.com

Education

2009–2013	University of Tartu, Bachelor of physics
2015–2017	Aalborg University, Master of nanobiotechnology
2021–...	University of Tartu, PhD student of biomedical engineering

Employment

2013–2018	Roosa gepard OÜ, software developer
2018–2019	Mercans OÜ, software developer
2019–2020	Carrumtech OÜ, software developer
2020–2021	Quretec OÜ, software developer

Scientific work

Main fields of interest:

- Software
- Drug delivery

ELULOOKIRJELDUS

Isikuandmed

Nimi:	Mart Ernits
Sünniaeg:	05.10.1989.
E-mail:	mart223@gmail.com

Haridus

2009–2013	Tartu ülikool, füüsika bakalaureus
2015–2017	Aalborgi ülikool, nanobiotehnolooogia magister
2021–...	Tartu ülikool, Biomeditsiinitehnoloogia doktorant

Teenistuskäik

2013–2018	Roosa gepard OÜ, programmeerija
2018–2019	Mercans OÜ, programmeerija
2019–2020	Carrumtech OÜ, programmeerija
2020–2021	Quretec OÜ, programmeerija

Teadustegevus

Peamised uurimisvaldkonnad:

- Tarkvara
- Ravimite kohaletoimetamine

DISSERTATIONES TECHNOLOGIAE UNIVERSITATIS TARTUENSIS

1. **Imre Mäger**. Characterization of cell-penetrating peptides: Assessment of cellular internalization kinetics, mechanisms and bioactivity. Tartu 2011, 132 p.
2. **Taavi Lehto**. Delivery of nucleic acids by cell-penetrating peptides: application in modulation of gene expression. Tartu 2011, 155 p.
3. **Hannes Luidalepp**. Studies on the antibiotic susceptibility of *Escherichia coli*. Tartu 2012, 111 p.
4. **Vahur Zadin**. Modelling the 3D-microbattery. Tartu 2012, 149 p.
5. **Janno Torop**. Carbide-derived carbon-based electromechanical actuators. Tartu 2012, 113 p.
6. **Julia Suhorutšenko**. Cell-penetrating peptides: cytotoxicity, immunogenicity and application for tumor targeting. Tartu 2012, 139 p.
7. **Viktoryia Shyp**. G nucleotide regulation of translational GTPases and the stringent response factor RelA. Tartu 2012, 105 p.
8. **Mardo Kõivomägi**. Studies on the substrate specificity and multisite phosphorylation mechanisms of cyclin-dependent kinase Cdk1 in *Saccharomyces cerevisiae*. Tartu, 2013, 157 p.
9. **Liis Karo-Astover**. Studies on the Semliki Forest virus replicase protein nsP1. Tartu, 2013, 113 p.
10. **Piret Arukuusk**. NickFects–novel cell-penetrating peptides. Design and uptake mechanism. Tartu, 2013, 124 p.
11. **Piret Villo**. Synthesis of acetogenin analogues. Asymmetric transfer hydrogenation coupled with dynamic kinetic resolution of α-amido-β-keto esters. Tartu, 2013, 151 p.
12. **Villu Kasari**. Bacterial toxin-antitoxin systems: transcriptional cross-activation and characterization of a novel *mqsRA* system. Tartu, 2013, 108 p.
13. **Margus Varjak**. Functional analysis of viral and host components of alphavirus replicase complexes. Tartu, 2013, 151 p.
14. **Liane Viru**. Development and analysis of novel alphavirus-based multifunctional gene therapy and expression systems. Tartu, 2013, 113 p.
15. **Kent Langel**. Cell-penetrating peptide mechanism studies: from peptides to cargo delivery. Tartu, 2014, 115 p.
16. **Rauno Temmer**. Electrochemistry and novel applications of chemically synthesized conductive polymer electrodes. Tartu, 2014, 206 p.
17. **Indrek Must**. Ionic and capacitive electroactive laminates with carbonaceous electrodes as sensors and energy harvesters. Tartu, 2014, 133 p.
18. **Veiko Voolaid**. Aquatic environment: primary reservoir, link, or sink of antibiotic resistance? Tartu, 2014, 79 p.
19. **Kristiina Laanemets**. The role of SLAC1 anion channel and its upstream regulators in stomatal opening and closure of *Arabidopsis thaliana.* Tartu, 2015, 115 p.

20. **Kalle Pärn**. Studies on inducible alphavirus-based antitumour strategy mediated by site-specific delivery with activatable cell-penetrating peptides. Tartu, 2015, 139 p.
21. **Anastasia Selyutina**. When biologist meets chemist: a search for HIV-1 inhibitors. Tartu, 2015, 172 p.
22. **Sirle Saul**. Towards understanding the neurovirulence of Semliki Forest virus. Tartu, 2015, 136 p.
23. **Marit Orav**. Study of the initial amplification of the human papillomavirus genome. Tartu, 2015, 132 p.
24. **Tormi Reinson**. Studies on the Genome Replication of Human Papillomaviruses. Tartu, 2016, 110 p.
25. **Mart Ustav Jr**. Molecular Studies of HPV-18 Genome Segregation and Stable Replication. Tartu, 2016, 152 p.
26. **Margit Mutso**. Different Approaches to Counteracting Hepatitis C Virus and Chikungunya Virus Infections. Tartu, 2016, 184 p.
27. **Jelizaveta Geimanen**. Study of the Papillomavirus Genome Replication and Segregation. Tartu, 2016, 168 p.
28. **Mart Toots**. Novel Means to Target Human Papillomavirus Infection. Tartu, 2016, 173 p.
29. **Kadi-Liis Veiman**. Development of cell-penetrating peptides for gene delivery: from transfection in cell cultures to induction of gene expression *in vivo*. Tartu, 2016, 136 p.
30. **Ly Pärnaste**. How, why, what and where: Mechanisms behind CPP/cargo nanocomplexes. Tartu, 2016, 147 p.
31. **Age Utt**. Role of alphavirus replicase in viral RNA synthesis, virus-induced cytotoxicity and recognition of viral infections in host cells. Tartu, 2016, 183 p.
32. **Veiko Vunder**. Modeling and characterization of back-relaxation of ionic electroactive polymer actuators. Tartu, 2016, 154 p.
33. **Piia Kivipõld**. Studies on the Role of Papillomavirus E2 Proteins in Virus DNA Replication. Tartu, 2016, 118 p.
34. **Liina Jakobson**. The roles of abscisic acid, CO_2, and the cuticle in the regulation of plant transpiration. Tartu, 2017, 162 p.
35. **Helen Isok-Paas**. Viral-host interactions in the life cycle of human papillomaviruses. Tartu, 2017, 158 p.
36. **Hanna Hõrak**. Identification of key regulators of stomatal CO_2 signalling via O_3-sensitivity. Tartu, 2017, 260 p.
37. **Jekaterina Jevtuševskaja**. Application of isothermal amplification methods for detection of *Chlamydia trachomatis* directly from biological samples. Tartu, 2017, 96 p.
38. **Ülar Allas**. Ribosome-targeting antibiotics and mechanisms of antibiotic resistance. Tartu, 2017, 152 p.
39. **Anton Paier**. Ribosome Degradation in Living Bacteria. Tartu, 2017, 108 p.
40. **Vallo Varik**. Stringent Response in Bacterial Growth and Survival. Tartu, 2017, 101 p.

41. **Pavel Kudrin**. In search for the inhibitors of *Escherichia coli* stringent response factor RelA. Tartu, 2017, 138 p.
42. **Liisi Henno**. Study of the human papillomavirus genome replication and oligomer generation. Tartu, 2017, 144 p.
43. **Katrin Krõlov**. Nucleic acid amplification from crude clinical samples exemplified by *Chlamydia trachomatis* detection in urine. Tartu, 2018, 118 p.
44. **Eve Sankovski**. Studies on papillomavirus transcription and regulatory protein E2. Tartu, 2018, 113 p.
45. **Morteza Daneshmand**. Realistic 3D Virtual Fitting Room. Tartu, 2018, 233 p.
46. **Fatemeh Noroozi**. Multimodal Emotion Recognition Based Human-Robot Interaction Enhancement. Tartu, 2018, 113 p.
47. **Krista Freimann**. Design of peptide-based vector for nucleic acid delivery in vivo. Tartu, 2018, 103 p.
48. **Rainis Venta**. Studies on signal processing by multisite phosphorylation pathways of the *S. cerevisiae* cyclin-dependent kinase inhibitor Sic1. Tartu, 2018, 155 p.
49. **Inga Põldsalu**. Soft actuators with ink-jet printed electrodes. Tartu, 2018, 85 p.
50. **Kadri Künnapuu**. Modification of the cell-penetrating peptide PepFect14 for targeted tumor gene delivery and reduced toxicity. Tartu, 2018, 114 p.
51. **Toomas Mets**. RNA fragmentation by MazF and MqsR toxins of *Escherichia coli.* Tartu, 2019, 119 p.
52. **Kadri Tõldsepp**. The role of mitogen-activated protein kinases MPK4 and MPK12 in CO_2-induced stomatal movements. Tartu, 2019, 259 p.
53. **Pirko Jalakas**. Unravelling signalling pathways contributing to stomatal conductance and responsiveness. Tartu, 2019, 120 p.
54. **S. Sunjai Nakshatharan**. Electromechanical modelling and control of ionic electroactive polymer actuators. Tartu, 2019, 165 p.
55. **Eva-Maria Tombak**. Molecular studies of the initial amplification of the oncogenic human papillomavirus and closely related nonhuman primate papillomavirus genomes. Tartu, 2019, 150 p.
56. **Meeri Visnapuu**. Design and physico-chemical characterization of metal-containing nanoparticles for antimicrobial coatings. Tartu, 2019, 138 p.
57. **Jelena Beljantseva**. Small fine-tuners of the bacterial stringent response – a glimpse into the working principles of Small Alarmone Synthetases. Tartu, 2020, 104 p.
58. **Egon Urgard**. Potential therapeutic approaches for modulation of inflammatory response pathways. Tartu, 2020, 120 p.
59. **Sofia Raquel Alves Oliveira**. HPLC analysis of bacterial alarmone nucleotide (p)ppGpp and its toxic analogue ppApp. Tartu, 2020, 122 p.
60. **Mihkel Örd**. Ordering the phosphorylation of cyclin-dependent kinase Cdk1 substrates in the cell cycle. Tartu, 2021, 228 p.
61. **Fred Elhi**. Biocompatible ionic electromechanically active polymer actuator based on biopolymers and non-toxic ionic liquids. Tartu, 2021, 140 p.

62. **Liisi Talas**. Reconstructing paleo-diversity, dynamics and response of eukaryotes to environmental change over the Late-Glacial and Holocene period in lake Lielais Svētiņu using sedaDNA. Tartu, 2021, 118 p.
63. **Livia Matt**. Novel isosorbide-based polymers. Tartu, 2021, 118 p.
64. **Koit Aasumets**. The dynamics of human mitochondrial nucleoids within the mitochondrial network. Tartu, 2021, 104 p.
65. **Faiza Summer**. Development and optimization of flow electrode capacitor technology. Tartu, 2022, 109 p.
66. **Olavi Reinsalu**. Cancer-testis antigen MAGE-A4 is incorporated into extracellular vesiclesand is exposed to the surface. Tartu, 2022, 130 p.
67. **Tetiana Brodiazhenko**. RelA-SpoT Homolog enzymes as effectors of Toxin-Antitoxin systems. Tartu, 2022, 132 p.
68. **Georg-Marten Lanno**. Development of novel antibacterial drug delivery systems as wound scaffolds using electrospinning technology. Tartu, 2022, 175 p.
69. **Liubov Cherkashchenko**. New insights into alphaviral nsP2 functions. Tartu, 2023, 171 p.
70. **Kristina Kiisholts**. Peptide-based drug carriers and preclinical nanomedicine applications for endometriosis treatment. Tartu, 2023, 138 p.
71. **Kai Rausalu**. Alphaviral nsP2 protease: From requirements for functionality to inhibition. Tartu, 2023, 175 p.
72. **Laura Sandra Lello**. Unraveling the intricate nature of the alphavirus RNA replicase. Tartu, 2023, 219 p.
73. **Houman Masnavi**. Visibility Aware Navigation. Tartu, 2023, 180 p.
74. **Kadir Aktas**. Cosmic Ray Tomography based Object Reconstruction and Recognition. Tartu, 2023, 104 p.
75. **Egils Avots**. Brain abnormality detection using statistical analysis of individual structural connectivity networks and EEG signals. Tartu, 2023, 223 p.
76. **Sainan Wang**. Structure-guided insights into the functions of CHIKV nsP2. Tartu, 2024, 154 p.
77. **Anneli Samel**. Unveiling the characteristics of cancer-testis antigen MAGEA10. Tartu, 2024, 136 p.
78. **Ikechukwu Ofodile**. Fault tolerant attitude control for nanosatellites: ESTCube-2 case. Tartu, 2024, 130 p.
79. **Olena Zamora**. Impacts of plant hormones on controlling stomatal conductance. Tartu, 2024, 166 p.
80. **Mariliis Hinnu**. *In vitro* methods for studying the mechanisms of ribosome-targeting antibiotics. Tartu, 2024, 143 p.
81. **Chung-Yueh Yeh**. Characterization of MPK and HT1 kinases in CO_2-induced stomatal movements. Tartu, 2024, 118 p.
82. **Iman Dadras**. Low power neural network-based control and actuation solutions for insect-scale robots. Tartu, 2024, 149 p.
83. **Fatemeh Rastgar**. Towards reliable real-time trajectory optimization. Tartu, 2024, 158 p.

84. **Maria Maloverjan**. Optimizing cell-penetrating peptide-based nanoparticles for delivery of nucleic acid therapeutics. Tartu, 2024, 172 p.
85. **Joonas Merisalu**. Resistive switching in memristor structures with multilayer dielectrics. Tartu, 2024, 149 p.
86. **Siim Laanesoo**. Novel high-performance biomass-based polymers. Tartu, 2024, 117 p.
87. **Henri Ingelman**. Systems-level characterisation and improvement of *Clostridium autoethanogenum* metabolism. Tartu, 2024, 164 p.
88. **Mailis Laht**. Using the One Health approach for mapping the spread of antibiotic resistant bacteria in Estonia. Tartu, 2024, 188 p.
89. **Ingrid Rebane**. Structure-property relationships of moldable silicone foams. Tartu, 2024, 164 p.
90. **Robert Valner**. Design of TeMoto, a software framework for dependable, adaptive, and collaborative autonomous robots. Tartu, 2024, 182 p.
91. **Kristiina Kurg**. Exploring the potential of a liquid biopsy approach for melanoma diagnostics and the role of extracellular vesicles in atherosclerosis development. Tartu, 2025, 201 p.
92. **Rauno Sedrik**. Synthesis and investigation of polymers from different cyclic bio-based monomers. Tartu, 2025, 155 p.
93. **Alina Ismagilova**. Safety assessment of novel bio-based polymers and compounds used in low carbon technologies. Tartu, 2025, 156 p.
94. **Baiba Brūmele**. Uncovering the TRMT112 methyltransferase network and characterising the cellular functions of TRMT112-network member N6AMT1. Tartu, 2025, 135 p.
95. **Ingmar Tulva**. Causes and consequences of stomatal density in relation to atmospheric humidity. Tartu, 2025, 142 p.
96. **Yauheni Sarokin**. Passive and active liquid mediation in natural and synthetic morphing systems. Tartu, 2025, 173 p.
97. **Hans Priks**. Life within 3D printed engineered living materials based on micellar hydrogels. Tartu, 2026, 126 p.
98. **Kaspar Koolmeister**. Stomatal CO_2 regulation pathway and its application for modulating tomato plants. Tartu, 2026, 118 p.